PLASTIC SHEAR PROPERTIES OF METALS AND ALLOYS AT HIGH STRAIN RATES

Mike C. Tsao, et al

Oxford University

Prepared for:

Air Force Materials Laboratory

19 March 1973

AD-770754

UNCLASSIFIED
Security Classification

DOCUMENT CONTROL DATA - R & D

(Security classification of title, body of abstract and indexing annotation must be entered when the overall report is classified)

1. ORIGINATING ACTIVITY (Corporate author) Department of Engineering Science, University of Oxford, Oxford, England	2a. REPORT SECURITY CLASSIFICATION Unclassified 2b.

3. REPORT TITLE

Plastic shear properties of metals and alloys at high strain rates

4. DESCRIPTIVE NOTES (Type of report and inclusive dates)

Scientific. Interim.

5. AUTHOR(S) (First name, middle initial, last name)

Mike C. Tsao and John D. Campbell

6. REPORT DATE	7a. TOTAL NO. OF PAGES	7b. NO. OF REFS
19 March 1973	83	18

8a. CONTRACT OR GRANT NO.	9a. ORIGINATOR'S REPORT NUMBER(S)
AFOSR-71-2056 b. PROJECT NO. 7351=06 c. 61101F d. 680100	AFML-TR-73-177 9b. OTHER REPORT NO(S) (Any other numbers that may be assigned this report)

10. DISTRIBUTION STATEMENT

Approved for public release, distribution unlimited

11. SUPPLEMENTARY NOTES	12. SPONSORING MILITARY ACTIVITY
Tech, other.	AIR FORCE MATERIALS LABORATORY (LLD) Wright-Patterson Air Force Base Ohio 45433

13 ABSTRACT

An account is given of experiments using a torsional split Hopkinson-bar apparatus, by means of which short tubular specimens can be subjected to shear strain rates up to 3000 sec^{-1}. The methods of calibration and data reduction are described, and static and dynamic shear properties are given for mild and stainless steel, titanium, copper, yellow brass and aluminium. Some of the results are compared with existing data obtained in shear, tension and compression tests on similar materials, and the significance of the observed rate dependence of the flow stress is briefly discussed.

DD FORM 1 NOV 1473

UNCLASSIFIED
Security Classification

UNCLASSIFIED
Security Classification

14 KEY WORDS	LINK A		LINK B		LINK C	
	ROLE	WT	ROLE	WT	ROLE	WT
Shear strength, strain-rate effects, Hopkinson Bar, mild steel, stainless steel, titanium, copper, aluminium						

*U.S.Government Printing Office: 1973 — 758-428/254

NOTICE

When Government drawings, specifications, or other data are used for any purpose other than in connection with a definitely related Government procurement operation, the United States Government thereby incurs no responsibility nor any obligation whatsoever; and the fact that the Government may have formulated, furnished, or in any way supplied the said drawings, specifications, or other data, is not to be regarded by implication or otherwise as in any manner licensing the holder or any other person or corporation, or conveying any rights or permission to manufacture, use, or sell any patented invention that may in any way be related hereto.

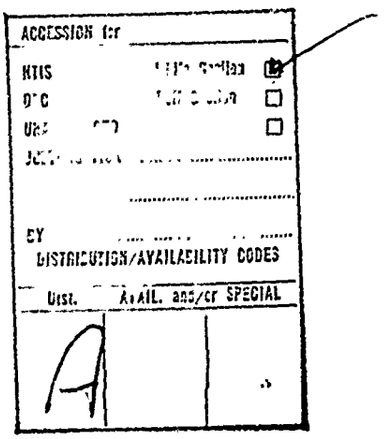

Copies of this report should not be returned unless return is required by security considerations, contractual obligations, or notice on a specific document.

i

10

AFML-TR-73-177

PLASTIC SHEAR PROPERTIES OF METALS AND ALLOYS AT HIGH STRAIN RATES

M. C. C. TSAO AND J. D. CAMPBELL

DEPARTMENT OF ENGINEERING SCIENCE
UNIVERSITY OF OXFORD

FOREWORD

This report was prepared by the Department of Engineering Science, University of Oxford, Oxford, England under AFOSR Grant No. 71-2056. This grant was initiated under Porject No. 7353, "Characterization of Solid Phase and Interphase Phenomena in Crystalline Substances", Task No. 735303, "Surface Effects and Mechanical Response". Funds for this project were supplied to the Air Force Materials Laboratory by the Office of Aerospace Research. The work was administered by the Metals and Ceramics Division, Air Force Materials Laboratory, Air Force Systems Command, Wright-Patterson Air Force Base, Ohio, with Dr. T. Nicholas, AFML/LLN, as Project Scientist.

This report covers work conducted from February 1971 to January 1973. Manuscript was released by the author on March 1973 for publication.

The work reported herein was initiated with the aid of Air Force Materials Laboratory DIRECTOR'S FUNDS.

This technical report has been reviewed and approved.

Vincent J. Russo

VINCENT J. RUSSO
ACTG. CHIEF, NDT & MECHANICS BRANCH
METALS & CERAMICS DIVISION

Abstract

An account is given of experiments using a torsional split Hopkinson-bar apparatus, by means of which short tubular specimens can be subjected to shear strain rates up to 3000 sec^{-1}. The methods of calibration and data reduction are described, and static and dynamic shear properties are given for mild and stainless steel, titanium, copper, yellow brass and aluminium. Some of the results are compared with existing data obtained in shear, tension and compression tests on similar materials, and the significance of the observed rate dependence of the flow stress is briefly discussed.

Table of Contents

List of Figures

1. Introduction

The use of a thin-walled tubular specimen subjected to pure torque has considerable advantages in determining the flow stresses of materials. These advantages are largely due to the absence of Poisson's-ratio effects which lead to necking or barrelling in tests under axial loading, and the consequent limitation on the strains that can be achieved. In dynamic tests, a further advantage is that inertial loading due to lateral expansion or contraction is avoided; assuming that wave effects within the specimen are negligible, the inertial loading is essentially zero at constant strain rate, whereas in tension or compression it increases with the square of the strain rate, thus setting an upper limit to the rates at which accurate data can be obtained (Klepaczko 1969, Samanta 1971).

A minor disadvantage of the torsion test is that the strain varies radially within the wall of the tube. However, for specimens of wall thickness equal to 10% of the mean radius the stress variation will amount to only a few percent for a typical ductile material in the work-hardening range, and the error due to neglect of this variation will be very small.

From a review of the available techniques of dynamic testing, Duffy et al. (1970) concluded that the most direct and convenient method for determining dynamic flow properties of materials is the split Hopkinson pressure-bar adapted for torsion. Two types of loading wave can be used in such an apparatus: a short duration pulse of approximately rectangular form, or a large duration pulse approximating to a step function. For given wave speeds and lengths of bar, the latter allows larger strains to be achieved, and it is employed in the present investigation.

In earlier work (Campbell and Dowling 1970, Lewis and Campbell 1972, Nicholas and Campbell 1972) various devices have been developed for obtaining steep-fronted torsional waves by means of the release of a pre-twisted elastic bar. This method has now been used to test a variety of metals and alloys,

as part of a research programme aimed at obtaining engineering data for these materials and also assessing the types of micro-mechanism governing their rate dependence. The present report gives dynamic shear stress-strain results for strain rates in the range 250 to 3000 sec^{-1}; these results are compared to those obtained at quasi-static strain rates, and to some of the existing data on similar materials.

2. Description of Apparatus

The apparatus was built on an 8 ft. long torsion machine bed, at one end of which was a motor and gear box giving four speeds ($3\frac{1}{3}$, 10, 30, 90 degrees/minute); at the other end was an Avery mechanical torquemeter. The general assembly is shown in Figure 2.1, and a schematic diagram of the mechanical and electrical apparatus is shown in Figure 2.2. A loading bar 27 in. in length was connected to the gear box, and a tubular specimen was connected between the loading bar and the recording bar of length 14.5 in. As seen in Fig. 2.1, this bar was made with a square nut at its far end, by which it could be gripped for calibration purposes. The diameter of the bars was 7/8 in. and the material was aluminium alloy (BS 1476, HE 15 WP) with a nominal 0.1% tensile proof stress of 58,000 psi. A frictional clamp was designed to hold a torque of 500 to 1300 in-lb by a high-strength notched steel bolt which tightened the clamp. Continued tightening of the notched bolt caused it to break, thus releasing the stored energy in the pre-twisted loading bar. As a result, a loading wave was sent down the bar and through the specimen into the recording bar. An unloading wave was simultaneously sent up the loading bar as shown in the (x, t) diagram of Figure 2.3.

Two sets of TML FCA-3 Rosette foil-type strain gauges were attached to the bar by CH- cement at two stations on the loading bar. Each set consisted of a pair of gauges forming a four-arm bridge, the two pairs being located at opposite sides of the bar to eliminate any bending signals. The output of one set of gauges was fed to a Sanborn 321 recorder and was used to indicate the total pre-loading torque applied. The output of the other set was fed to a Tektronix 551 dual-beam oscilloscope and gave the input-wave amplitude. In order to eliminate undesired bending effects due to tightening the clamp, a frame incorporating two bearings in the loading-bar section and two bearings in the recording bar section was provided. These bearings were accurately machined with brass foil shielding the aluminium bar, and were aligned with

a stainless steel bar before being fixed to the bed of the machine.

Since the signal in the recording bar was small for weak specimen materials, four pairs of gauges were located at one cross-section, positioned 90 degrees apart around the recording bar. This set of gauges gave twice the magnification of the input set. The specimen was glued to the bars by CN-cement - an acetone soluble cement. The CN-cement joint could hold a torque of more than 250 in-lb which was sufficient to yield the specimen. The advantage of using the CN-cement was its instantly drying property, which permitted many tests per day.

All gauges outputs were first fed to a switch box, to which Farnell E30-type stabilized-voltage supplies and a resistance box were also connected. With known shunt resistances, all gauges were calibrated to give the corresponding torques. From the switch box, the inputs were fed to the D-type plug-in units which gave differential outputs. These differential outputs were in turn fed to the 1A1 plug-in units in the Tektronix 551 oscilloscope which had 4-cm maximum beam deflections.

The trigger system consisted of a spring made of a thin metal strip, which was placed across the clamp and formed part of an electrical circuit. When the clamp bolt broke, the spring lost contact with the clamp to break the circuit and thus trigger the oscilloscope; the circuit is shown in Figure 2.4(a) and the spring strip in position on the clamp in Fig. 2.4(b).

The specimen materials were supplied in the form of rods of 1 in. diameter. The specimens were first machined to a nominal size, and after being heat-treated they were measured by a travelling microscope, at least two readings being obtained for each dimension; the average of these readings was used in the calculation of the results.

3. Calibration

3.1 Static Calibration

Static calibration was done in three independent ways:

(a) A known torque was gradually applied at the end of the recording bar by means of dead-weight loading on a lever arm. The recording and loading bars were connected together and the end of the loading bar was fixed at the gear box. Both clockwise and counterclockwise torque measurements were performed.

(b) A torque was applied at the end of the loading bar by means of the motor and gear system ($3\frac{1}{3}$ degrees/min), while the end of the recording bar was balanced by dead weights on the lever arm. Both clockwise and counterclockwise measurements were performed.

(c) A torque was applied at the end of the loading bar by means of the motor and gear system ($3\frac{1}{3}$ degrees/min) while the end of the recording bar was connected to the mechanical torquemeter. Hence the torque was obtained directly from reading the calibrated dial on this meter. Both clockwise and counterclockwise measurements were performed.

3.2 Calculation of Torque by Shunt Resistance

Since one set of gauges form a four-arm bridge, a variable shunt resistance box was used to simulate the strain in the gauges, as shown in Figure 3.1. The voltage change ΔV across the bridge is directly proportional to the normal strain ε as shown in Figure 3.1(a) and is inversely proportional to the shunt resistance R_c as shown in Figure 3.1(b), for $R_c >> r$. The torque T is directly proportional to the strain ε, and the strain is inversely proportional to the shunt resistance. Hence the torque is inversely proportional to the shunt resistance, i.e. $T = C/R_c$, C being a constant which was determined by the following tests.

Each set of gauges was tested by connecting it to a Sanborn recorder. The deflection on the Sanborn recorder corresponding to each torque applied

to the bar was then balanced by adjusting the shunt resistance. Taking average readings for the clockwise and counterclockwise tests, which eliminated the friction involved in the bearings, consistent relationships between torque and calibration resistance were obtained. The torques (in-lb) expressed in terms of shunt resistance (KΩ) for the three gauges were found to be as follows:

$$\text{Static gauge} \quad T_0 = \frac{20.5 \times 10^3}{R_c}$$

$$\text{Input gauge} \quad T_1 = \frac{17.5 \times 10^3}{R_c}$$

$$\text{Output gauge} \quad T_2 = \frac{35 \times 10^3}{R_c}$$

3.3 Dynamic Calibration

(a) By switching in the shunt resistance, a simulated torque in the bar was expressed in terms of the deflection of the oscilloscope or of the Sanborn recorder. The sensitivity of the oscilloscope was set to 0.05 V/Div* and the time scale was set to 50 μsec/Div. The reference resistance for the input gauge was R_c = 45 KΩ which gave the corresponding torque $T_1 = \frac{17.5 \times 10^3}{45}$ = 388 in-lb. For the output gauge R_c = 102 KΩ, the torque T_2 was $\frac{35 \times 10^3}{R_c}$ = 343 in-lb. The results are shown in Figure 3.2.

(b) A dummy specimen was cemented between the loading bar and the recording bar. A pre-loading torque was applied to the loading bar by means of the motor and gear system; this torque (T_0) was measured by the Sanborn recorder. The corresponding calibration resistance was 660 KΩ so that $T_0 = \frac{20.5 \times 10^3}{660}$ = 311 in-lb.

As the bolt in the friction clamp broke, half of the total pre-

---

* 1 Division = 1 cm on the oscilloscope screen.

loading torque, i.e. $T_0/2$, was sent down the bar. This torque was first recorded by the input gauge as T_1 and through the dummy specimen was again recorded by the output gauge as T_2. The resulting trace is shown in Figure 3.3. It was found that T_1 = 149.5 in-lb and T_2 = 146 in-lb.

(c) In this test the error was $(T_1 - T_2)/T_1$ = 3.5/149.5 = 2.3%.

(d) In all tests the pre-loading torques were recorded on the Sanborn recorder, and the values of T_0 and $2T_1$ were compared. It was found that for all tests $(T_0 - 2T_1)/T_0$ was within 5%. For this particular test the error is $(T_0 - 2T_1)T_0$ = (311 - 299)/311 = 3.9%.

The differences between T_0 and $2T_1$, T_1 and T_2 were due to friction losses in the bearings.

(e) Dynamic calibrations by inserting shunt resistances were performed on each gauge immediately before and after each test.

4. Bending and Static Tests

4.1 Bending Test

The shear-wave speed and bending-wave speed for propagation along a bar are approximately of the same magnitude. Hence, to eliminate bending effects is an important requirement in dynamic shear tests. The following procedures were used to check the amount of bending present.

A dial gauge was set on top of the bar near the clamp to indicate the maximum deflection of the bar; the apparatus was adjusted so that this was less than 0.002 in. during tightening of the clamp. Two bending gauges were placed on the dummy specimen, and using the same sensitivity for both channels of the oscilloscope, the bending stresses were recorded separately in two perpendicular directions during two dynamic shear tests. The results are shown in Figure 4.1, and it is clear that the bending stress is negligible compared to the shear stress.

4.2 Static Test

The end of the recording bar was made to have a square nut so that it could be fixed to the machine bed or connected to the Avery torque meter. In a static test, with the specimen cemented between the loading and recording bar, the end of the recording bar was fixed to the bed, and the end of the loading bar was twisted by the motor and gear box at $3\frac{1}{3}$ degrees/min. The static gauge on the loading bar was connected to the Sanborn recorder which recorded the total torque on the bar and the time. The time gave the total angle of twist of the bars and the specimen, i.e. the sum of the elastic deformation of the loading and recording bars and the elasto-plastic deformation of the specimen. Thus, the shear strain of the specimen was obtained from the total angle of twist by subtracting the elastic twist due to the bars; this twist was obtained by repeating the test after replacing the specimen by a dummy specimen, that is, a short bar, one inch long, of the same material and the same diameter as the loading and recording bars. The mean shear stress in

the specimen wall was obtained by the formula $T/2\pi r_m^2 t_k$, where T is the torque recorded by Sanborn recorder, r_m is the mean radius of the tubular specimen, and t_k is the thickness of the specimen. The dimensions of the loading and recording bars and the specimen are shown in Figure 4.2.

5. Reduction of Data

5.1 One-Dimensional Torsional Wave Theory

The elementary theory of torsional wave propagation was used to calculate the dynamic stress-strain relationship for the specimen. This theory neglects end effects due to the change of cross section area between the specimen gauge length and the bars; however, an exact analysis* shows that these effects are negligible for pulses such as those occurring in the present tests. According to the elementary theory, the relationship between torque and angular velocity for a unidirectional wave is as follows:

$$T = J\rho c\omega$$

where T = torque (ft-lb, Nm)

d = diameter of the loading and recording bar (ft., m)

J = polar moment of inertia of the bar cross-section (ft^4, m^4)

ρ = density of the bar ($slug/ft^3$, kg/m^3)

c = shear wave speed along the bar (ft/sec, m/sec)

$J\rho c$ = torsional impedance of the bar (ft^2-slug/sec, kgm^2/sec)

ω = angular velocity of the bar (sec^{-1}).

The input wave approaches the specimen with a torque T_1 ; T_2 is the amount of torque transmitting through the specimen, and $(T_2 - T_1)$ is the amount of torque that reflects at the specimen and loading bar interface back into the loading bar. This torque is negative since the interface is almost a free end. The angular velocity at this interface is found by subtracting the reflected torque from the input torque and dividing by the torsional impedance of the bar. The relationship is therefore as follows:

$$\omega_1 = \frac{T_1 - (T_2 - T_1)}{J\rho c} = \frac{2T_1 - T_2}{J\rho c} .$$

The angular velocity at the interface of the specimen with the recording bar is:

$$\omega_2 = T_2/J\rho c .$$

---

* Campbell & Tsao, 1972.

Since the specimen is short, the waves acting on both ends of the specimen can be considered to occur at the same time. This gives the difference of the angular velocities as

$$\Delta\omega = 2(T_1 - T_2)/J\rho c .$$

The average shear strain rate in the specimen is then given by

$$\dot{\gamma} = \Delta\omega r_m/\ell .$$

The shear strain γ is obtained by integration:

$$\gamma = \int_0^t \dot{\gamma} dt = (r_m/\ell) \int_0^t \Delta\omega \, dt .$$

The relationships of shear rate, shear strain and time are illustrated in Figure 5.1. The average stress in the specimen is as given before:

$$\tau = T_2/2\pi r_m^2 t_k .$$

5.2 Numerical Values

The numerical values for the bars (diameter d) are as follows:

$d = 7/8$ in. $= 0.0729$ ft. $= 0.0222$ m.

$J = \frac{\pi}{32} d^4 = 0.0576 \text{ in}^4 = 2.78 \times 10^{-6} \text{ ft}^4 = 2.40 \times 10^{-8} \text{ m}^4.$

$\rho = 0.10 \text{ lb/in}^3 = 5.37 \text{ slug/ft}^3 = 2.77 \times 10^3 \text{ kg/m}^3.$

$c = 0.125 \text{ in/ sec} = 1.04 \times 10^4 \text{ ft/sec} = 3.175 \times 10^3 \text{ m/sec.}$

$J\rho c = 0.1553 \text{ ft}^2\text{-slug/sec} = 0.211 \text{ kgm}^2/\text{sec.}$

If the torques are measured in in-lb units, the equations become:

$$\Delta\omega = 1.07 (T_1 - T_2) \text{ rad/sec,}$$

and

$$\dot{\gamma} = 1.07(r_m/\ell)(T_1 - T_2) \text{ sec}^{-1}.$$

6. Dynamic Test Results

6.1 Mild Steel EN2A

(a) Preparation of Specimens

The specimens were annealed in a vacuum furnace, at pressure of 1.5×10^{-4} mm Hg, at 750°C for 2 hours and furnace cooled. The dimensions of the specimen were measured by a travelling microscope after heat treatment. The chemical composition (wt. %) of the steel was as follows:

C	Mn	Si	S	P	Ni	Cr	Mo	Cu	O_2	N_2
0.075	0.40	0.005	0.018	0.025	0.11	0.02	0.018	0.08	0.012	0.004

(b) Torque - Time Records

Typical dynamic torsion test records for mild steel EN2A are shown in Figure 6.1.1. The first trace is the input torque which had a rise time about 25 μsec. The input pulse lasted about 180 μsec before the reflected wave arrived at the gauge position. At about 105 μsec after the wave arrived at the input gauge, the transmitted wave arrived at the recording gauge; this wave lasted 200 μsec before the arrival of the wave reflected from the end of the recording bar. The end of the bar had a square nut integral with it, so that a positive incremental torsional wave was reflected there, as shown on the trace. The locations of the strain gauges and the clamp were so designed that the specimen was subjected to torsional straining for the same length of time as that indicated by the recording gauge trace (see Figure 2.3). During this interval of time the input torque at the specimen is approximately constant. In the calculation the duration of the recording signal was used.

After the tests, the microstructure of a few specimens was examined. A typical micrograph of the specimen is shown in Figure 6.1.2. It shows a uniform microstructure with a mean ferrite grain density of 689 grains/mm^2.

(c) Stress - Strain Curves

By using the equations given in section 5, the torque-time curves were

converted into strain rate-time, stress-time and stress-strain relationships. The strain rates were integrated with respect to time to obtain the strain by finite-difference and Simpson's-rule methods. The engineering shear stress and engineering shear strain relationships from the steel tests are shown in Figure 6.1.3. The engineering shear strain rates covered in the dynamic tests were from 900 sec^{-1} to 2700 sec^{-1}. The quasi-static test was performed at 0.0042 sec^{-1}. The upper yield stress from the quasi-static test is 18,000 psi. The corresponding lower yield is at 17,000 psi at a strain of ~2%. At the strain rate 2700 sec^{-1} the upper yield is at 51,000 psi and the lower yield is at 39,500 psi. The strain of the lower yield at this strain rate is ~8%. The strain at the lower yield point increases as the shear strain rate increases. After the lower yield strain, the work-hardening curve appeared to be of the same slope for all dynamic and static tests at the same shear strain.

(d) Strain Rate - Strain Curves

Typical curves showing shear strain rate as a function of shear strain are plotted in Figure 6.1.4. It is seen that the strain rate at 2700 sec^{-1} became essentially constant at a shear strain of approximately 8%; the corresponding strain at 1300 sec^{-1} was approximately 6%. These strains are roughly equal to the respective lower yield point strains. It is also seen that during the initial elastic straining the strain rate increases rapidly with increase of the shear strain. During the interval between upper yield and lower yield, the rate of increase of strain rate decreases with the increase of strain. After the lower yield point the material work-hardens at nearly constant shear strain rate.

(e) Stress - Strain Rate Curves

In Figure 6.1.5 the shear stress is plotted in terms of the logarithm of shear strain rate for constant shear strains between 10% and 40%. From this figure, a significant increase of stress is seen between the strain rates of 10^2 and 10^4 sec^{-1}. The results are in good agreement with those obtained by

Campbell and Lewis (1969) for the same material in torsional tests, as shown in Figure 6.1.6.

In order to permit comparison with results of tension tests, the von Mises yield criterion may be assumed, according to which the tensile stress σ, strain ε and strain rate $\dot{\varepsilon}$, are related to the shear stress τ, strain γ and strain rate $\dot{\gamma}$ by the equations

$$\tau = \sigma/\sqrt{3}\ , \quad \gamma = \sqrt{3}\varepsilon \quad \text{and} \quad \dot{\gamma} = \sqrt{3}\dot{\varepsilon}\ .$$

Fig. 6.1.6 shows the results of tensile tests at low and medium rates (Campbell and Cooper 1966) converted in this way, σ being taken as the nominal or engineering stress at $\varepsilon = 11.5\%$ ($\gamma = 20\%$). To permit precise comparison of these data with the present results, it would be necessary to convert the stresses to true values, and to take into account the differences in grain size and composition of the two materials. From the Hall-Petch relation

$$\sigma = \sigma_i + k_y d^{-\frac{1}{2}}\ ,$$

where d is the mean grain size and $k_y = 0.74\ \mathrm{MNm}^{-3/2}$ for steel (Armstrong 1968), the tensile yield stress of the material tested by Campbell and Cooper is expected to be about $63\ \mathrm{MN/m}^2$ (9.1 kpsi) higher than that of the present material. However, the lower carbon content (0.045%) and the reduction of cross sectional area during extension effectively compensate for this increase, so that the stress values at strains from $\varepsilon = 12\%$ to $\varepsilon = 24\%$ correspond closely to those measured at $\gamma = 20\%$ in the present tests.

The lower yield stresses obtained in various other tests are compared with the present results in Fig. 6.1.7 and it is seen that there is general agreement; however, the rate sensitivity at high rates is found from the present results to be nearly an order of magnitude greater than that at lower rates. This is believed to indicate that viscous damping effects are becoming important in controlling dislocation motion at these rates.

A similar increase in rate sensitivity is shown by the results of shear tests on specially shaped specimens (Campbell and Ferguson 1970), although this increase occurred at somewhat higher strain rates.

6.2 Mild Steel EN2D

(a) Preparation of Specimens

The specimens were annealed in a vacuum furnace, at a pressure of 1.5 x 10^{-4} mm Hg and a temperature of 700°C, for 4 hours and furnace cooled. The dimensions of the specimens were measured with a travelling microscope after heat treatment. The chemical composition of the steel was as follows (wt. %):

C	Mn	Si	S	P	Ni	Pb
0.082	1.07	0.03	0.255	0.065	0.14	0.005

Microscopic examination showed that the grain density was in the range 190-260 grains/mm^2, i.e. considerably lower than that of the EN2A steel; however, there were still 7 or 8 grains across the wall thickness of the specimen, and more than 3000 in the cross-sectional area.

(b) Torque - Time Records

Typical torque-time records are shown in Figure 6.2.1. Due to a slight malfunction in the release of the clamp when the bolt broke, the input torque curve is not flat after the rise time. However, the variation of the input torque does not significantly affect the general yielding and strain-hardening behaviour of the material, since the variation of the specimen strain rate is not large. The recording torque shows a distinct upper yield point and a lower yield strain which is followed by a deformation showing strong work-hardening. The pulse rise at the end of the recording signal was again due to the wave reflected from the square nut at the end of the recording bar.

(c) Stress - Strain Curves

The shear-stress vs. shear-strain relationships are shown in Figure 6.2.2. The curves show the strong work-hardening effect. The lower yield stress in the quasi-static test was 14,500 psi at a shear strain of about 1%, and with increase of shear strain rate the yield stress increased and the corresponding yield strain increased as shown by the dashed line in Figure 6.2.2.

(d) Strain Rate - Strain Curves

The variation in the strain rate during the dynamic tests is shown in Figure 6.2.3. At a nominal strain rate of 1500 sec^{-1}, for example, the rate was 1550 sec^{-1} at a strain of 5% which corresponds to the lower yield stress; after the lower yield strain the strain rate increased to 1775 sec^{-1} at a strain of 10%; the rate then decreased to 1500 sec^{-1} at a strain of 20%, and to 1200 sec^{-1} at a strain of 30%. The amount of variation in shear strain rate depends on the variation of $T_1 - T_2$, i.e. the difference of the input and recording-bar torques. T_2 shows a drop followed by an increase during the strain-hardening process, while T_1 shows an inverse variation. The nominal strain rate was taken as the average value for each test.

(e) Stress - Strain Rate Curves

The strain-rate sensitivity of mild steel EN2D is shown in Figure 6.2.4. In this figure, the stress is plotted against the true strain rate for strains of 5, 10, 20 and 30%. For example, in the test at a nominal strain rate of 1500 sec^{-1}, the stress of 64 kpsi in the strain-hardening region corresponds to a strain of 30%, when the true strain rate was 1200 sec^{-1}. The figure also shows that the stress increases significantly when the strain rate is greater than about 10^2 sec^{-1}. In fact the material starts to show significant rate sensitivity at a strain rate of 1 sec^{-1}.

(f) Effect of Grain Size on Lower Yield Stress

The specimens tested at nominal strain rates of 900 and 1200 sec^{-1} were found to have mean grain-size parameters ($d^{-\frac{1}{2}}$) of 3.7 and 4.0 $mm^{-\frac{1}{2}}$ respectively. The lower yield stresses for these specimens are plotted in Figure 6.2.5, together with the value obtained at a mean strain rate of 2700 sec^{-1} for the EN2A steel. Also plotted in the figure are lines derived from the tension tests of Campbell and Harding (1960) for nearly pure iron. These lines have been determined by using the von Mises relationships given on the figure; it is seen that they agree reasonably well with the present data, after

allowance is made for the difference in quasi-static yield strength, which is caused by the higher impurity content of the present material.

(g) Comparison of Results for Iron and Mild Steels

Figure 6.2.6 shows a comparison of the rate sensitivity of the EN2D steel with those obtained by Yen and Yew (1969) for iron and by Tsubouchi and Kudo (1968) for a mild steel, both from torsional tests. Due to the limitations of the apparatus used, a small range of strains was covered, but within this range the data are in good agreement with the present results.

The variation of lower yield stress with strain rate is shown in Figure 6.2.7, for EN2A and EN2D. It is seen that the rate sensitivity increases significantly for both materials at a strain rate of 10^3 sec^{-1}, the sensitivity being greater for EN2D than for EN2A.

The rate sensitivities of the flow stresses of the two steels are compared in Figure 6.2.8. The rate sensitivities of the EN2A and EN2D increase significantly at rates of about 10^3 and 10^2 sec^{-1} respectively, this difference probably being due to the difference in grain size. At low strain rates (<1 sec^{-1}), little difference in the rate sensitivities is found.

6.3 Titanium

(a) Preparation of Specimens

Commercially pure titanium was received as rods 1 in. in diameter. After the specimens were machined to the nominal size (Fig. 4.2), they were annealed in a vacuum furnace at 700°C for two hours, where the pressure was kept at 1.5×10^{-4} mm Hg. An approximate spectrographic analysis of the material showed that the specimen contained less than 0.1% of each of the elements Fe, Mn and Si. The dimensions of the specimen were measured individually with a travelling microscope after heat treatment. Each specimen was cleaned with acetone before it was attached to the testing bars with CN-cement. After test, the microstructure was photographed and is shown in Fig. 6.3.1; it consists of equi-axed grains of α phase, there being about 10

grains across the specimen thickness.

(b) Torque - Time Records

Typical oscillograms are shown in Fig. 6.3.2. The input torque T_1 rose from zero to its full magnitude in about 25 μsec. Due to the incomplete release of the clamp, the input torque continued to increase slightly after the rise time. The output torque shows a clear yield point though no yield drop, which is followed by a nearly linear work hardening curve. The output torque lasted about 180 μsec before the reflected wave arrived at the recording-bar gauges.

(c) Stress - Strain Curves

The shear-stress vs. shear-strain curves for different strain rates are shown in Fig. 6.3.3. The strain rates covered in the dynamic tests were between 250 sec^{-1} and 2000 sec^{-1}. A clear strain-rate dependence is seen in the figure, the dynamic stresses being much higher than the stress in quasi-static tests at 0.0043 sec^{-1}. The dynamic yield stress at the strain rate of 1250 sec^{-1} is more than twice that in the quasi-static test.

The yield point becomes more marked as the strain rate is increased, and at the highest rate (2000 sec^{-1}), an approximately constant work-hardening rate is reached soon after yield. In general, however, the work-hardening rate at large strains is little affected by strain rate.

(d) Strain Rate - Strain Curves

The variation of strain rate with strain in the dynamic tests is shown in Fig. 6.3.4. Since the input torques were slightly increasing and the rate of work hardening after yield was not large, the strain rates in these tests were fairly constant during plastic straining, except at a mean rate of 250 sec^{-1}, when the strain rate increased rapidly to its maximum value and then decreased gradually to its final value. In Fig. 6.3.3, the dashed line indicates the strains at which approximately constant rates were reached.

(e) Stress - Strain Rate Curves

The stress vs. strain rate curves for constant shear strains are shown in Fig. 6.3.5. It is clear that the (logarithmic) rate sensitivity at rates of the order of 10^3 sec^{-1} is considerably greater than that at lower rates, though in the absence of data at intermediate rates the exact rate dependence cannot be determined. However, the data of Nicholas and Whitmire (1970) for annealed 50-A titanium tested in shear show that at rates between 10^{-3} and 25 sec^{-1} the rate sensitivity is constant and approximately independent of strain. Results for a strain of 10%, taken from their report, are plotted in Fig. 6.3.5 and it is seen that the rate sensitivity is slightly less than that indicated by the present data. The higher absolute stress level may be attributed to the greater grain density (1100 to 3000 gr/mm^2) of the material tested by Nicholas and Whitmire.

6.4 Stainless Steel

(a) Preparation of Specimens

The stainless steel (EN58B) was received as rods 1 in. in diameter. This material is an austenitic 18 Cr/8 Ni steel similar to AISI 321, having the following specification (wt. %):

C	Si	Mn	S	P
<0.15	>0.20	<2.00	<0.045	<0.045

Specimens were machined to the nominal size (Fig. 4.2), and their dimensions measured with a travelling microscope. No further heat treatment was carried out on these specimens. Araldite cement was used to connect the specimen to the testing bars; this required at least 24 hours curing before the tests were performed.

(b) Torque - Time Records

Two oscillograms for the stainless steel are shown in Fig. 6.4.1. The recording-bar traces show some fluctuations during the strain-hardening process. The reasons for these disturbances are unknown, and in some tests

smooth curves were obtained. In analysing the data, an average curve through the fluctuations was used. From the traces it is seen that the stainless steel had an approximately linear strain-hardening region following the yield point.

(c) Stress - Strain Curves

The shear-stress vs. shear-strain curves are plotted in Fig. 6.4.2. The strain rate ranged from 0.0043 sec^{-1} to 2100 sec^{-1}. It is seen that all the data lie within a zone of 10% in stress deviation. The static-test curve is at the bottom of this zone and gives a yield stress of 48 kpsi. The mean yield stress for the dynamic tests appears to be approximately 50 kpsi. The strain-hardening curves for all the dynamic tests had the same slope. From this figure, it is apparent that stainless steel 321 EN58B has a small rate sensitivity.

(d) Strain Rate - Strain Curves

The variation of the strain rate with strain is shown in Fig. 6.4.3. By comparing the results shown in Fig. 6.4.2 with those of Fig. 6.4.3, it is seen that at the yield strain of about 0.8%, the strain rate had not yet reached its final value. After the yield point, the material began its strain-hardening process while the strain rate was increasing, until about 3% strain where it became approximately constant. It is seen in Fig. 6.4.2 that between the shear strains 0.8% and 3%, the slope of the curve in each test is flatter than the slope at strains greater than 3%. Due to the strain hardening and a roughly constant input torque, the strain rate decayed as the strain increased.

(e) Stress - Strain Rate Curves

The stress, as a function of strain rate at constant strain, is shown in Fig. 6.4.4. It is seen that the stress is almost constant for strain rates from 10^{-3} sec^{-1} to 10^{3} sec^{-1}. In the neighbourhood of 10^{3} sec^{-1}, the stress appears to decrease with increasing rate, though this may be due to scatter in the data. However, it is interesting to note that Baruch, Rosen

and Bodner (1968) found that stainless steel shows discontinuous yielding under certain conditions when the strain-rate sensitivity is negative. Such an inverse rate effect could therefore explain the fluctuations on the torque-time traces found in the present tests.

6.5 Copper

(a) Preparation of Specimens

Commercially pure copper was received as rods 1 in. in diameter. After the specimens were machined to the nominal size (Fig. 4.2), they were annealed in a vacuum furnace at 550°C for 24 hrs. at a pressure of 1.5×10^{-4} mm Hg and furnace cooled. The precise dimensions of each specimen were measured by a travelling microscope after heat treatment. CN-cement was used to connect the specimens to the testing bars. The chemical composition of the copper was as follows (wt. %):

Ag	Bi	Fe	Ni	O	Pb	Sn
0.002	0.0002	0.0005	0.001	0.029	0.0005	0.002

The high-conductivity copper is 96.48% in purity, but it should be noted that the copper is not an oxygen-free copper.

After test, the microstructure of one specimen was examined, and the grain density was found to be 1320 gr/mm^2. The grain structure is uniform, as shown in Fig. 6.5.1.

(b) Torque - Time Records

Typical oscillograms for copper in the dynamic shear tests are shown in Fig. 6.5.2. Due to the imperfect release of the fractional clamp, the input torque curve was again not as flat as was intended. The deviations in the input torque depended on the breaking conditions of the notched bolt, and they were found to be negligible when the input torque was large. This seems to indicate that they are of an approximately constant magnitude, independent of the clamping torque; their cause may be an unsymmetrical release of the clamp. The clamping torques for the copper tests were between 530

and 1325 in.lb. The output traces shown in the figure indicate that the copper did not have a marked yield point, but had a strong strain-hardening process.

(c) Stress - Strain Curves

The shear-stress vs. shear-strain curves for copper in the static and dynamic tests are shown in Fig. 6.5.3. The static test was at a strain rate of 0.0043 sec^{-1} and the strain rates in the dynamic tests were between 1125 sec^{-1} and 3000 sec^{-1}. The static stress was found to be lower than the dynamic stress for the corresponding shear strains, as shown in the figure. The dynamic stress points lie in a band of stress deviation 1 kpsi about the average line through the whole band. The dynamic over-stress increases with the increase of shear strain. For example, at the shear strain of 10%, the shear stress was 8 kpsi in the static test; at the same strain, the dynamic shear stress ranged from 10 kpsi for the rates between 1125 sec^{-1} and 3000 sec^{-1}, so the average dynamic over-stress was 3 kpsi. At a shear strain of 20%, however, the dynamic shear stresses were from about 14 kpsi to 16 kpsi for the same range of strain rates, and the average dynamic over-stress was 7 kpsi.

(d) Strain Rate - Strain Curves

Curves of strain rate vs. strain for all the dynamic tests on copper are shown in Fig. 6.5.4. It is seen that the nominal strain rates were reached at strains increasing from 1 or 2% at the lowest rate to 6 or 7% at the highest rate. In the early stages of straining, therefore, the strain rate was increasing rapidly.

(e) Stress - Strain Rate Curves

In Fig. 6.5.5, the stresses at three constant shear strains, 5%, 10% and 20%, are shown for the quasi-static rate of 0.0043 sec^{-1} and for strain rates of the order of 10^3 sec^{-1}. The slope of the stress versus log strain rate curve increases quite rapidly with increasing strain.

(f) Comparison with Existing Data

Dynamic tests on copper have been performed by many investigators. In Fig. 6.5.6, three sets of results are plotted. The compression results of Kolsky and Douch (1962) and of Lindholm (1964) have been converted into shear stress and shear strain by the von Mises relations shown in the figure; also, the equivalent shear strain rates for Lindholm's tests were calculated from the relation $\dot{\gamma} = \sqrt{3}\dot{\varepsilon}$. The stresses obtained by Lindholm were considerably lower than those obtained by Kolsky and Douch.

Baker and Yew (1966) performed shear tests on copper at strain rates between 4×10^{-4} and 2100 sec^{-1}. The range of dynamic shear strains was only from about 10% to 20%.

From the figure, it is seen that a precise comparison among all these tests is difficult. The data corresponding to the same strain rates do not agree well for the same strains, though the data for each investigation are consistent in that the static stress is lower than the dynamic stress at any given strain. The discrepancies could be caused by differences in impurity content and in grain size of the materials tested.

6.6 Yellow Brass

(a) Preparation of Specimens

The alloy was received in the form of 1 in. diameter rods, the specimens were machined and their precise dimensions measured. The specimens were cleaned with acetone before being attached to the testing bars by CN- cement. No heat treatment was carried out. The chemical composition of brass was analyzed spectrographically and found to be as follows (wt. %):

Al	As	Bi	Cu	Fe	Mg	Mn	Ni	P
0.01	0.02	0.002	64	0.4	0.005	0.02	0.2	0.02

Pb	Sb	Si	Sn	Ti	Zn
0.1	0.005	0.01	0.2	0.005	35

After test, a specimen was etched in a solution of alcoholic ferric chloride and the microstructure was examined. The result is shown in Fig. 6.6.1, from which it appears that the alloy contained an appreciable amount of the β phase, indicating a non-equilibrium condition.

(b) Torque - Time Records

Figure 6.6.2 shows two typical oscillograms for brass. The rise time of the input signal was about 20 μsec, after which the input torque was almost constant until the wave was reflected from the end of the input bar. The output signal arrived 104 μsec after the input signal. It is seen that the brass has a fairly definite yield point, followed by strain hardening at a relatively small rate compared to that of copper. Immediately after the test shown in Fig. 6.6.2(a), the oscilloscope was manually triggered to produce two base lines. In Fig. 6.6.2(b), the oscilloscope was triggered once before the test and once after the test. It is seen that the trace on the output channel drifted slightly. This slow drift did not affect the result, however, because the duration of the test is only 0.4 millisecond.

(c) Stress - Strain Curves

The shear-stress vs. shear-strain curves for the various nominal strain rates are plotted in Fig. 6.6.3, the dynamic rates ranging from 800 sec^{-1} to 2500 sec^{-1}. In the static test, the shear stresses are lower than those in the dynamic tests at the same shear strains. The yield stress in the static test is 22 kpsi, while the yield stress at the shear rate of 2500 sec^{-1} is 31 kpsi. In this figure, we can see clearly the differences among all the dynamic tests. This shows a significant rate sensitivity for the brass, though it is not large compared to that of pure B.C.C. metals. It is interesting to consider the curve for 2500 sec^{-1}. The stress increased to the yield point and plastic flow then started with a small strain-hardening rate; at larger strains the work-hardening rate increased. The material yielded at the shear strain of 2% where the shear strain rate was at about

1500 sec^{-1} and was still in the process of increasing (see below).

(d) Strain Rate - Strain Curves

The variations of shear strain rate during each dynamic test are shown in Fig. 6.6.4. For the test at a nominal rate of 2500 sec^{-1}, the rate did not become nearly constant until the strain reached 10%. Hence, the stress-strain curve shown in Fig. 6.6.3 can be studied in two parts. The first part consists of the elastic straining, yielding and the early plastic straining part; during this part of the deformation, the strain rate was continuously increasing. The second part is the work-hardening curve corresponding to plastic flow at approximately constant strain rate. Thus the increase in the slope of the curve at a strain of about 10% seems to be direct evidence of the rate sensitivity of the material.

(e) Stress - Strain Rate Curves

The rate sensitivity of the brass at three different shear strains, 10%, 20% and 30%, is shown in Fig. 6.6.5. The results of dynamic tests at the strain rates of 800 sec^{-1} to 2500 sec^{-1} are compared with those of the static test at 0.0043 sec^{-1}. It appears that the brass increases its flow stress linearly with increase of the logarithm of the strain rate, though there is some indication that the rate sensitivity is greater at the highest rates; the rate sensitivity is also seen to increase with strain.

6.7 Aluminium

(a) Preparation of Specimens

Commercially pure aluminium was received in the form of 1 in. diameter rods, from which specimens were machined, annealed in a vacuum furnace at 350°C for two hours and furnace cooled. The specimens were cleaned with acetone before being attached to the testing bars with CN- cement. The chemical composition of one specimen was analyzed after test. The results showed a purity of 99.74%, the composition being as follows (wt. %):

Cr	Cu	Fe	Ga	Mg	Mn	Ni	Si	Zn
0.001	0.001	0.18	0.01	0.002	0.001	0.001	0.06	0.007

(b) Torque - Time Records

Typical oscillograms for aluminium are shown in Fig. 6.7.1. It is seen that the output signal is fairly small, but with the available equipment, the use of the foil gauges, and the size of the specimen, this was the maximum amplitude that could be used at the time of testing. It is seen that there is a fairly well defined yield point followed by work hardening at a decreasing rate.

(c) Stress - Strain Curves

The shear-stress vs. shear-strain curves for both static and dynamic tests are shown in Fig. 6.7.2. In the static test, the specimen gauge length was 0.1 in., that is, twice the length used for the other materials in the static tests; hence, the strain rate for the static test was half as large. The dynamic tests covered strain rates from 600 sec^{-1} tO 2800 sec^{-1}. The static yield stress of the aluminium is about 2 kpsi, while the yield stress at a strain rate of 2200 sec^{-1} is about 4 kpsi. The dynamic over-stress is larger at larger shear strains, rising to about 5 kpsi at 40% strain; the percentage increase in flow stress rises from about 50% at 5% strain to 80% at 40% strain.

(d) Strain Rate - Strain Curves

The variation of strain rate during each test is shown in Fig. 6.7.3. In the test at a nominal rate of 600 sec^{-1}, the rate became constant at a strain of 3%, while in the test at a nominal rate of 2800 sec^{-1}, the rate became constant at a strain of 6%. Thus a constant rate of straining was only reached after the specimen had been strained well into the work-hardening region.

(e) Stress - Strain Rate Curves

The rate sensitivity of aluminium can be seen from Fig. 6.7.4, in which

the shear stresses at three different shear strains (10%, 20% and 30%) are plotted against the logarithm of the strain rate. The rate sensitivity (assumed constant over the range of rates covered) increases with strain.

The present data for a strain of 10% are compared with those obtained by Campbell and Dowling (1970), Klepaczko (1968), and Campbell and Lewis (1969) in Fig. 6.7.5. The rate sensitivity given by the present data is higher than that of Campbell and Dowling but lower than that of Klepaczko and about the same as that obtained by Campbell and Lewis. Differences in the absolute stress levels are presumably due to the differences in purity and possibly heat treatment.

7. Discussion and Conclusions

The work described in the present report was undertaken to exploit the advantages of the torsional split Hopkinson-bar apparatus as a means of determining the mechanical properties of materials at large strains and strain rates. It has been shown that the method can produce consistent results for a wide variety of metals and alloys, at mean strain rates in the range 10^2 to 10^4 sec^{-1}. At the higher rates, shear strains up to 50% have been attained. In cases where comparison with earlier work is possible, good general agreement has been found; it is considered, therefore, that the way is open for a systematic study of the effect of factors such as temperature, pre-straining and microstructure on the dynamic flow behaviour of materials. Such a study should throw light on the operative micromechanisms of plastic flow, in addition to giving useful information for the formulation of macroscopic constitutive relations.

The results presented in Section 6 show that all the materials tested are to some degree rate-sensitive, but that in general the increase in flow stress between strain rates of order 10^{-3} and 10^3 sec^{-1} is less than 100%. Such a relatively weak dependence indicates that the logarithm of the strain rate is more appropriate than the rate itself as a measure of the speed of deformation, and this in turn suggests the applicability of thermal-activation rate theory. According to this theory, the (plastic) strain rate is given by

$$\dot{\gamma} = \dot{\gamma}_o \exp(-\Delta G/kT) ,$$

where $\dot{\gamma}_o$ is the maximum rate that could theoretically be achieved if all the available elementary deformation processes were activated,

ΔG is the free activation energy of activation,

k is Boltzmann's constant,

and T is the absolute temperature.

The observed logarithmic rate dependence of the flow stress can thus be interpreted as being caused by the stress dependence of ΔG . Defining the

rate dependence as

$$\mu = (\partial\tau/\partial \ell n \dot{\gamma})_T ,$$

where τ is the macroscopic flow stress, it follows that

$$\frac{1}{\mu} = \left(\frac{\partial \ell n \dot{\gamma}_o}{\partial \tau}\right)_T + \frac{V^*}{nkT} ,$$

where $V^* \cong -n(\partial \Delta G/\partial \tau)_T$, the activation volume,

and n is a factor which relates the applied shear stress to the critical resolved shear stress.

Assuming that $\dot{\gamma}_o$ does not vary by more than say an order of magnitude as the stress increases due to changing the strain rate by a factor of 10^6, the value of μ gives a direct indication of the activation volume V^*. This quantity is a measure of the size of the elementary deformation mechanism. For F.C.C. metals, in which this mechanism is believed to be the intersection of dislocations (Seeger 1955, 1956), V^* is expected to depend on the dislocation density and thus to decrease as the plastic strain increases; for B.C.C. and H.C.P. metals, however, a stress dependence is likely since lattice friction (the Peierls force) is thought to be important.

A full comparison of experiment with theory requires the measurement of μ as a function of stress, strain and temperature; since in the present work temperature was not a variable, such a comparison is not yet possible. However, the results of Figs. 6.5.5 and 6.7.4 indicate that for the F.C.C. metals copper and aluminium μ does increase with increasing strain, at constant temperature. This is in agreement with the results of various other investigators obtained in compression tests, which have been compared in a recent review (Campbell 1973). Using the von Mises relations to convert from shear to compression, the slopes of the lines plotted in Figs. 6.5.5 and 6.7.4 correspond to rate sensitivities rather greater than those determined from compression tests on similar materials, but the differences are probably not significant.

Fig. 6.6.5 shows rate sensitivities for yellow brass which are about twice those of copper at the same strains; this difference may be accounted for by the presence of (non-equilibrium) B.C.C. ß-phase grains. The general stress level is of course raised by alloying with zinc, though the work-hardening rate is little affected (see Figs. 6.5.3 and 6.6.3).

The results for the mild steels are in good agreement with data obtained by other workers (see Figs. 6.1.6 and 6.1.7). They show that the rate sensitivity of the lower yield stress is roughly constant up to a strain rate of about 10^3 sec^{-1}, but that of the flow stress increases continuously with increasing stress or strain rate. Such an increase could be due to a stress-dependent activation volume, or to a variation in the mobile dislocation density which governs $\dot{\gamma}_o$. At the highest rates, the rate sensitivity of the lower yield stress increases sharply, as found by earlier workers (see Campbell and Ferguson 1970). The stress-strain curves (Figs. 6.1.3 and 6.2.2) show a marked yield drop and a yield strain which increases with strain rate. Differences in the general stress level and in the work-hardening rate seem to be associated with grain-size variation, rather than differences in composition (see Fig. 6.2.5).

The rate sensitivity of titanium (Fig. 6.3.5) is essentially independent of strain, its value at rates up to 10^3 sec^{-1} being about an order of magnitude greater than those of copper and aluminium. At rates above 10^3 sec^{-1} there seems to be a considerable increase in rate sensitivity. As pointed out in section 6.3(e), the results are generally consistent with those of Nicholas and Whitmire, the small difference probably being due to variation in grain size. The rate sensitivity below 10^3 sec^{-1} is comparable to that found from compression tests on a Ti 6Al 4V alloy containing both H.C.P. α-phase and B.C.C. ß-phase (Lindholm and Bessey 1969). Fig. 6.3.3 shows that the work-hardening rate decreases rapidly with increasing strain at low strain rate, while at high rates it is nearly constant after yield.

Results for stainless steel (Figs. 6.4.2 and 6.4.4) show a small rate sensitivity, comparable to that of copper, which is essentially independent of strain. There is some indication of a negative rate sensitivity at high rates, which has been discussed in section 6.4(e). The work-hardening rate is unaffected by strain rate.

It should be pointed out that no account has been taken of adiabatic heating of the specimen during the dynamic tests. Such heating will normally reduce the flow stress at large strains and hence the isothermal work-hardening rate will be greater than that indicated in the plotted curves. For the same reason the rate sensitivity at large strains would be greater under isothermal conditions. The evaluation of these effects will be undertaken when data are available at temperatures other than ambient.

The considerable increase in rate sensitivity which has been observed in mild steel and titanium tested at the highest rates may be caused by a change in rate-controlling mechanism. This phenomenon requires further investigation using even higher strain rates and tests over a range of temperatures.

Acknowledgements

Mr. R. C. Stone and Mr. R. Sawala assisted in carrying out the metallographic examination of the specimens. Financial assistance for the project of which this work forms a part was provided by the Science Research Council.

References

Baker, W. E. and Yew, C. H. 1966 J. Appl. Mech. 33, 917.

Campbell, J. D. 1973 Mat. Sci. and Eng.

Campbell, J. D. and Dowling, A. R. 1970 J. Mech. Phys. Solids 18, 43.

Campbell, J. D. and Ferguson, W. G. 1970 Phil. Mag. 21, 63.

Campbell, J. D. and Harding, J. 1960 Response of Metals to High Velocity Deformation (Eds. Shewmon, P. G. and Zackay, V. F.) Interscience, New York, 51.

Campbell, J. D. and Tsao, M. C. C. 1972 Quart. J. Math. Appl. Mech. 25, 173.

Duffy, J., Campbell, J. D. and Hawley, R. H. 1970 J. Appl. Mech. 38, 83.

Klepaczko, J. 1968 J. Mech. Phys. Solids, 16, 255.

Klepaczko, J. 1969 Report 17/1969, Inst. Fundamental Tech. Res., Polish Academy of Sciences.

Kolsky, H. and Douch, L. S. 1962 J. Mech. Phys. Solids, 10, 195.

Lewis, J. L. and Campbell, J. D. 1972 Exp. Mech. 12, 520.

Lindholm, U. S. 1964 J. Mech. Phys. Solids, 12, 317.

Lindholm, U. S. and Bessey, R. L. 1969 Tech. Rept. AFML-TR-69-119, Air Force Materials Laboratory, Wright-Patterson Air Force Base, Ohio.

Nicholas, T. and Campbell, J. D. 1972 Exp. Mech. 12, 441.

Nicholas, T. and Whitmire, J. N. 1970 Tech. Rept. AFML-TR-70-218, Air Force Materials Laboratory, Wright-Patterson Air Force Base, Ohio.

Samanta, S. K. 1971 J. Mech. Phys. Solids, 19, 117.

Seeger, A. 1955 Phil. Mag. 46, 1194.

Seeger, A. 1956 Dislocations and Mechanical Properties of Crystals (Eds. Fisher, J. C., Johnston, W. G., Thomson, R., and Vreeland, T. Jr.) Wiley, New York, 243.

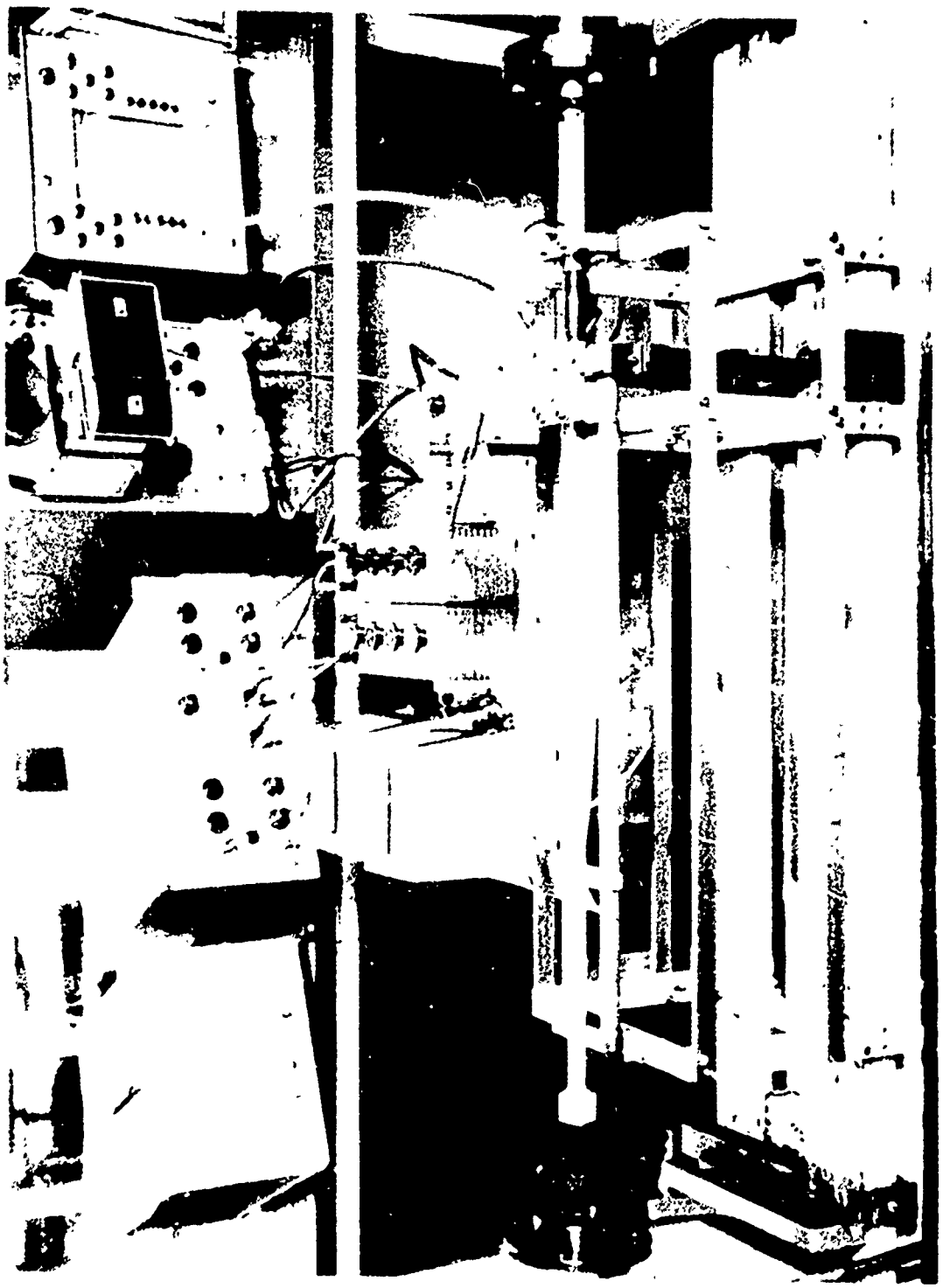

Fig. 2.1 General view of apparatus

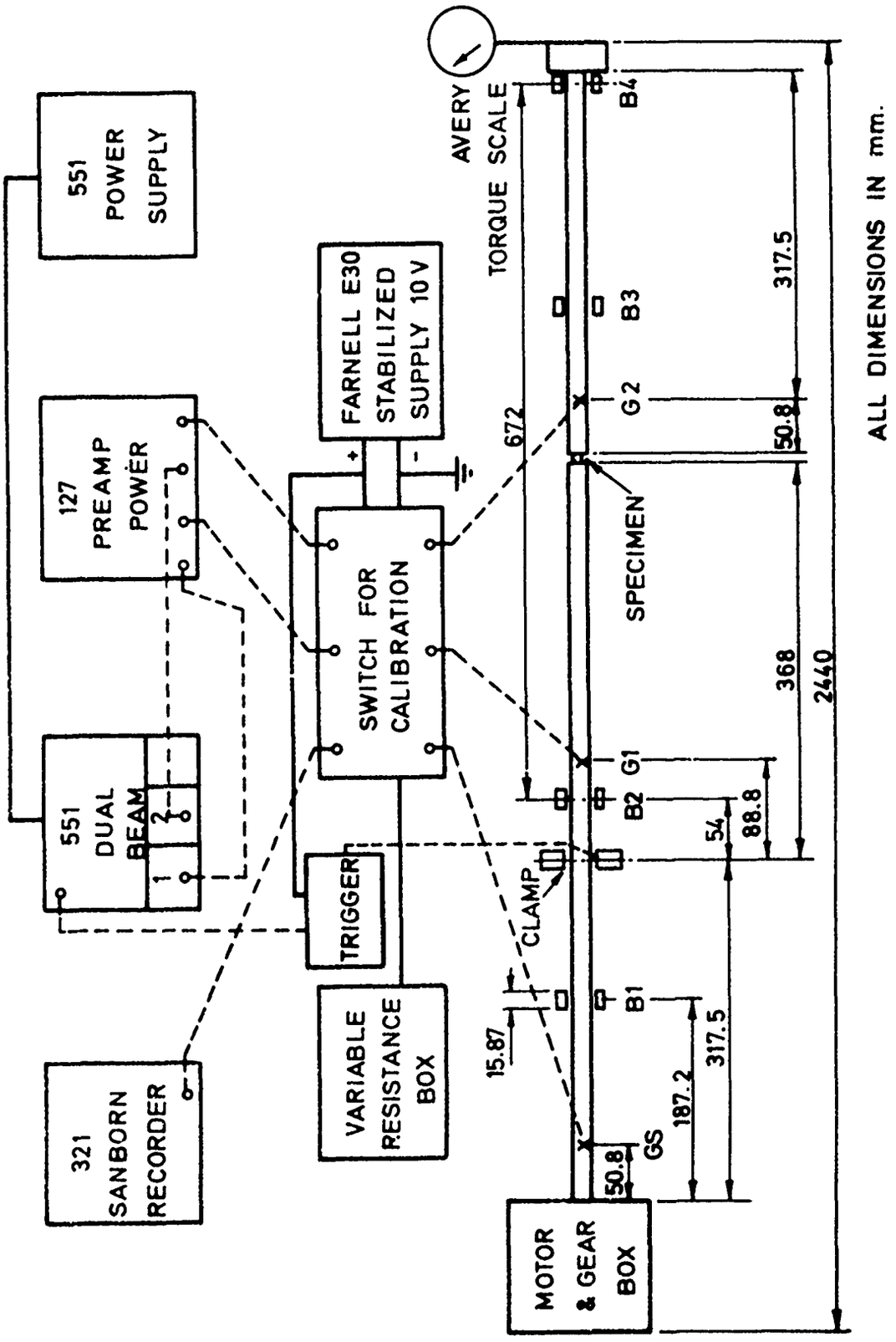

Fig. 2.2 Schematic mechanical and electrical layout

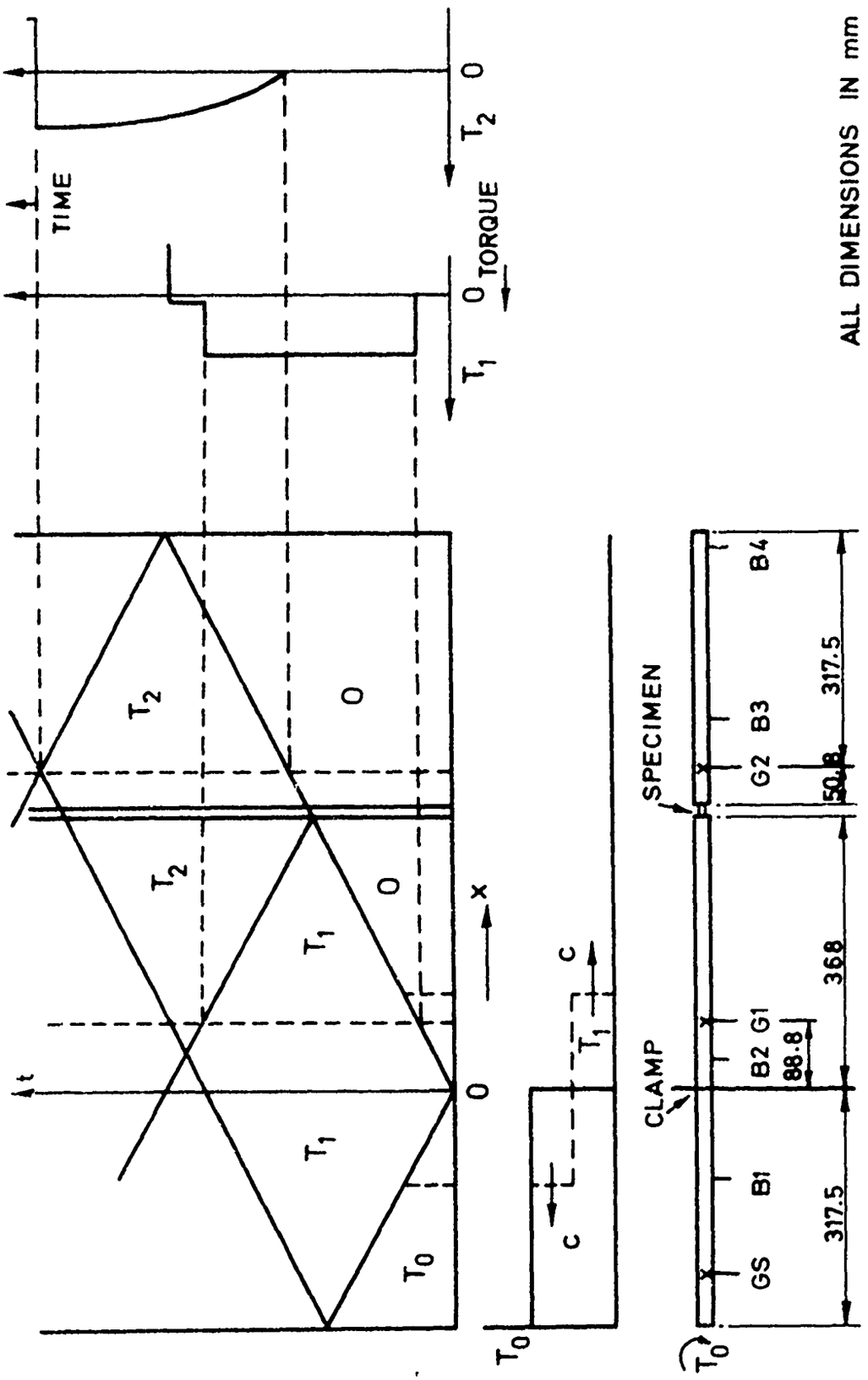

Fig. 2.3 Illustrating wave propagation and recording

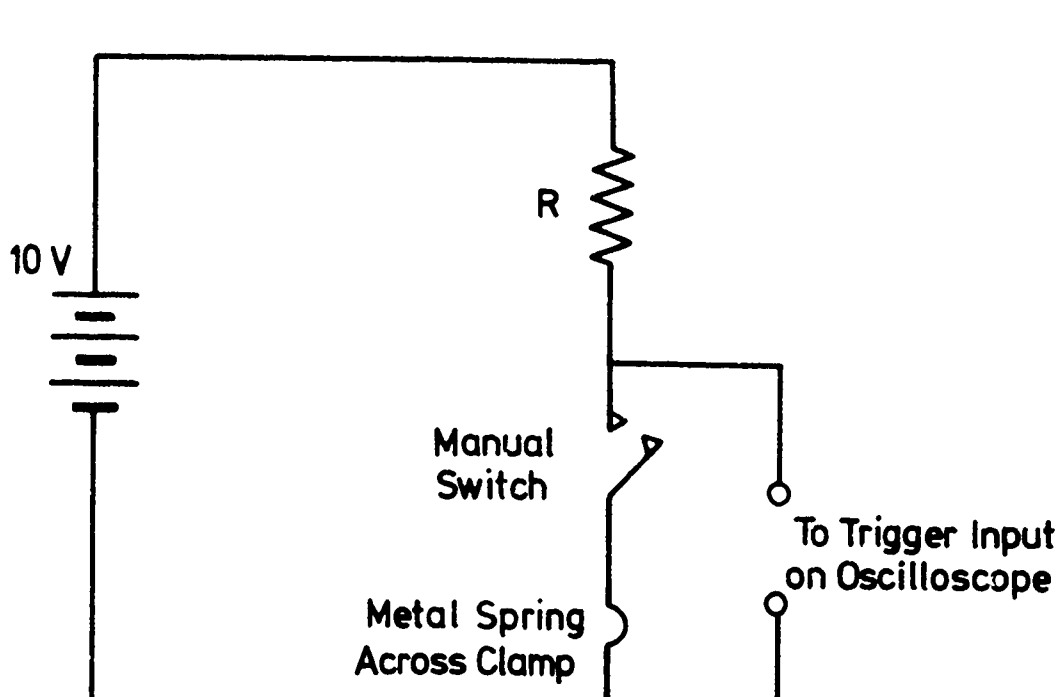

Fig. 2.4(a) Trigger circuit

Fig. 2.4(b) View of clamp and trigger spring switch

a) Torsional Strain

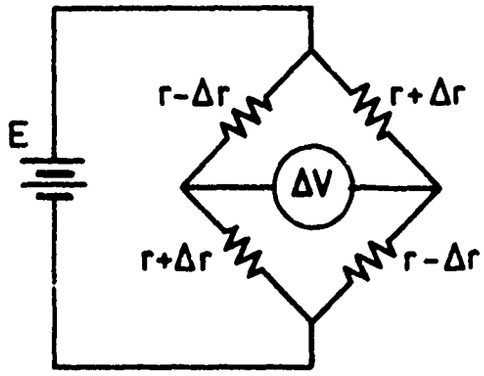

r = Gauge resistance

Δr = Change of resistance

E = D.C. Voltage supply

ΔV = Change of voltage

$\Delta r/r = \Delta V/E$

ε = Normal strain = $\Delta \ell/\ell$

ℓ_o = Original length of gauge

$\Delta \ell_o$ = Change of length

S = Gauge factor $\dfrac{\Delta r/r}{\Delta \ell_o/\ell_o} = \dfrac{\Delta V/E}{\varepsilon}$

$\varepsilon = \Delta V/ES$

γ = Engineering shear strain = 2ε

T = Torque = $(4G \frac{J}{d})\varepsilon$

J = Polar moment of inertia of the bar

G = Shear modulus

d = Bar diameter

$T = (4G \frac{J}{d} \frac{1}{ES})\Delta V$

b) Shunt Resistance

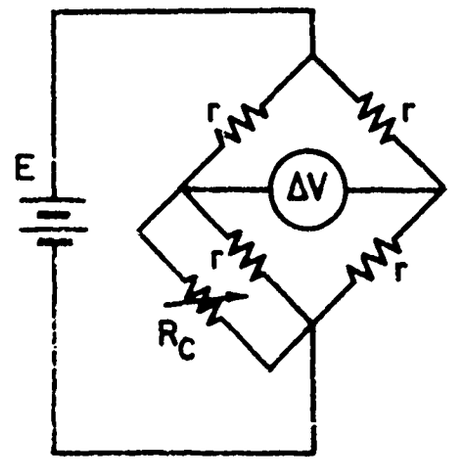

$\Delta V = \dfrac{E}{4} \cdot \dfrac{r}{R_C}$

$T = \dfrac{C}{R_C}$, where

C = GJr/Sd

Fig. 3.1 Gauge bridge circuits

Oscilloscope Sensitivity 0.05 V/Div for both Channels

(a) Input gauge $T_1 = 17.5 \times 10^3 / R_c$

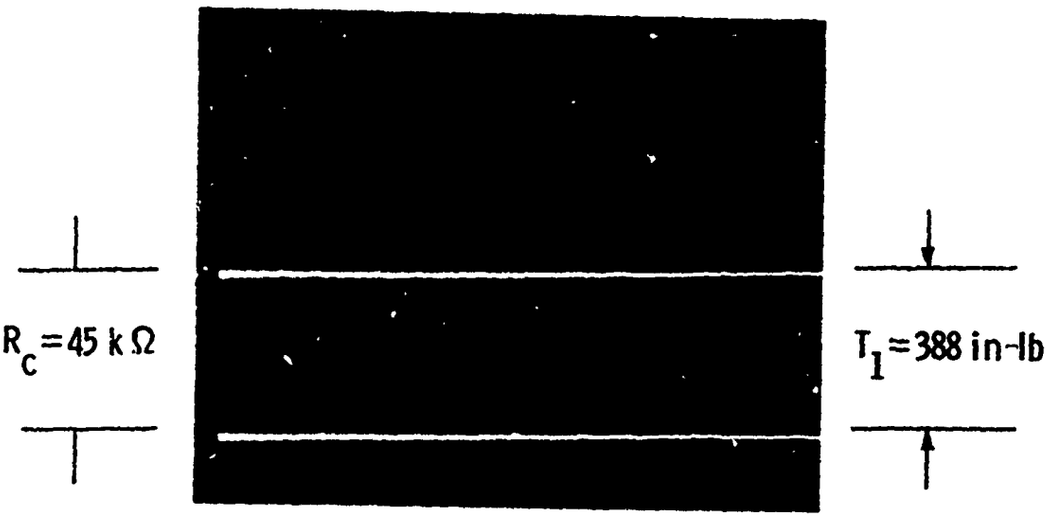

(b) Output gauge $T_2 = 35 \times 10^3 / R_c$

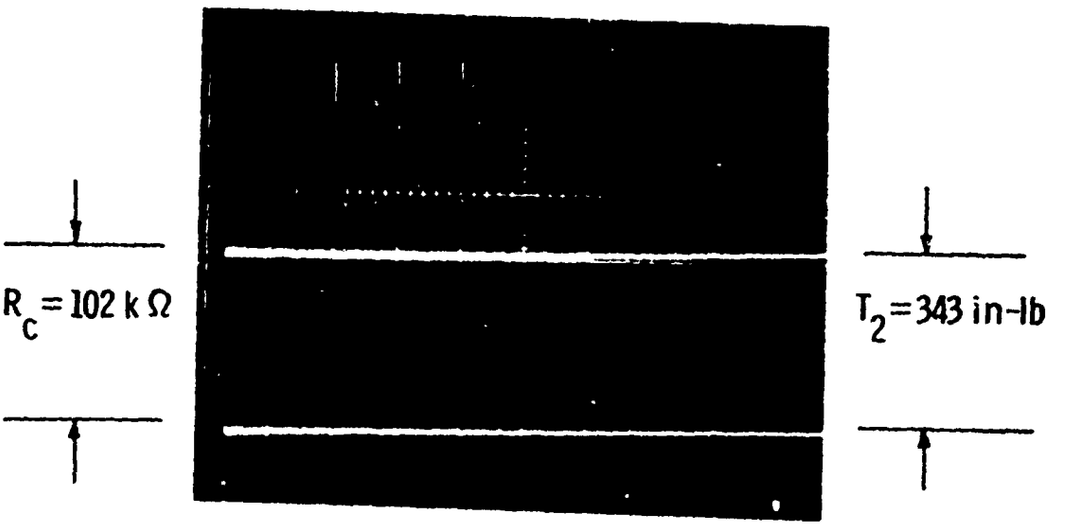

Fig. 3.2 Oscilloscope calibration traces

Oscilloscope Sensitivity 0.05 V/Div for both Channels

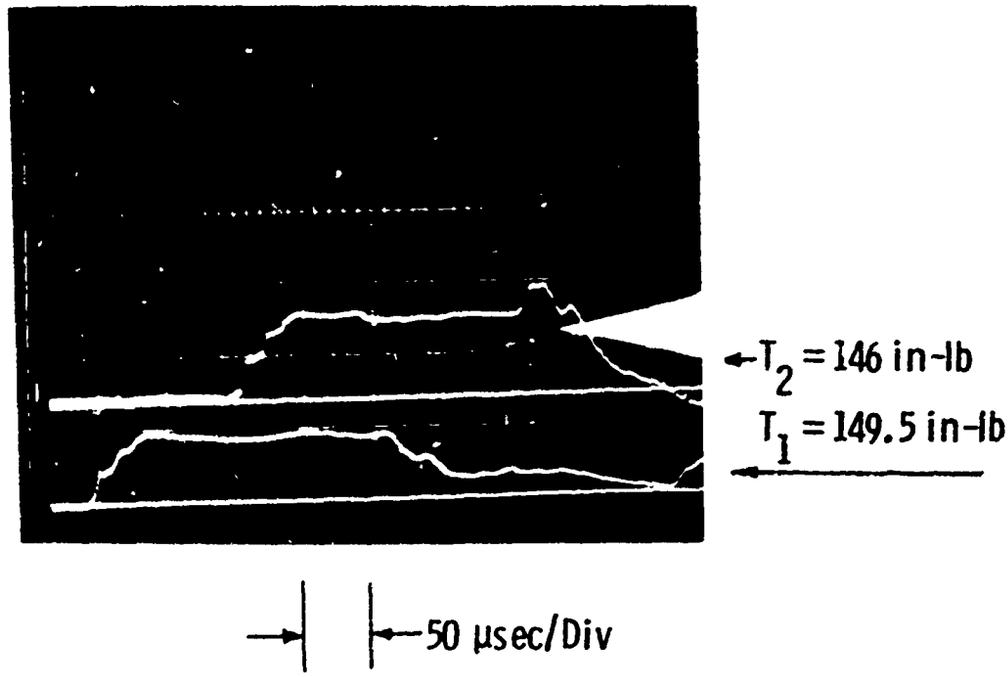

Fig. 3.3 Dynamic test of the system with a dummy specimen cemented between loading and recording bar

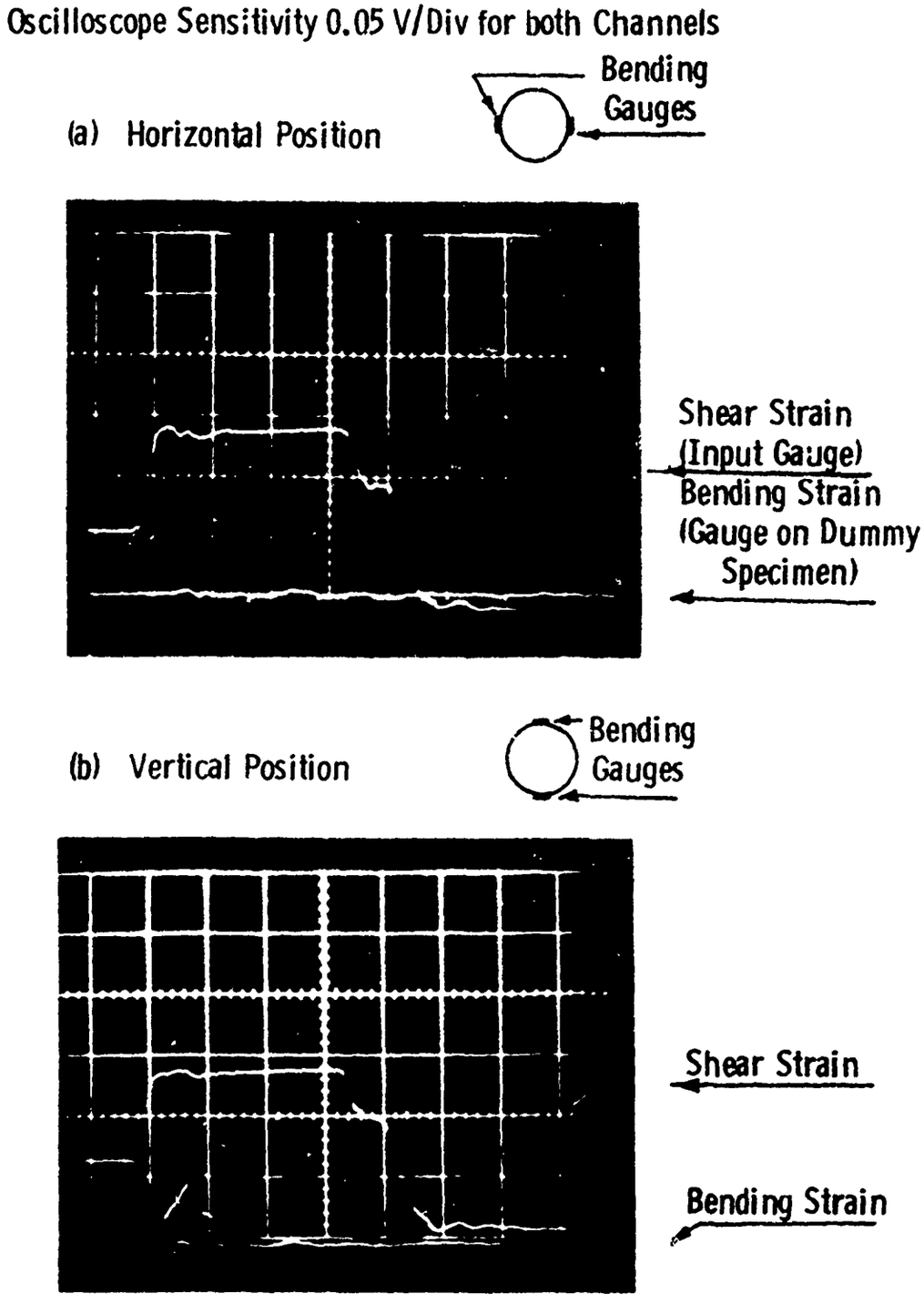

Fig. 4.1 Comparison of torsion and bending waves

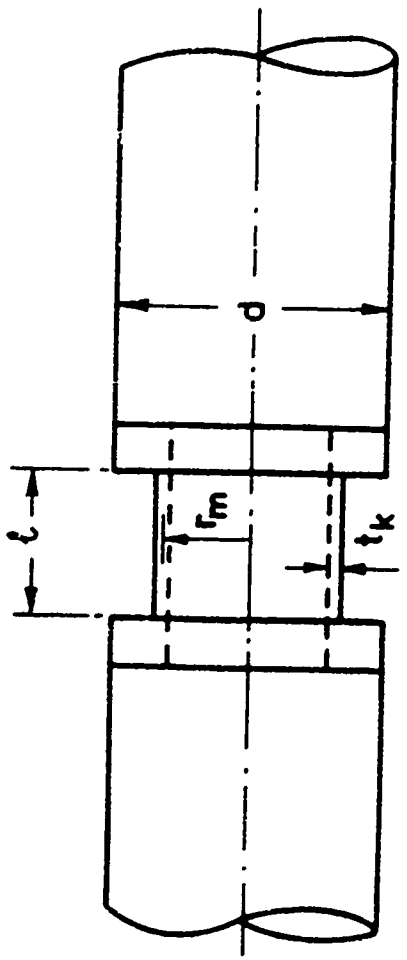

$d = 7/8$ in.
$t_k = 0.020$ in.
$\ell = 0.125$ in. and 0.25 in.
$r_m = 0.20$ in.

Fig. 4.2 Nominal dimensions of specimen

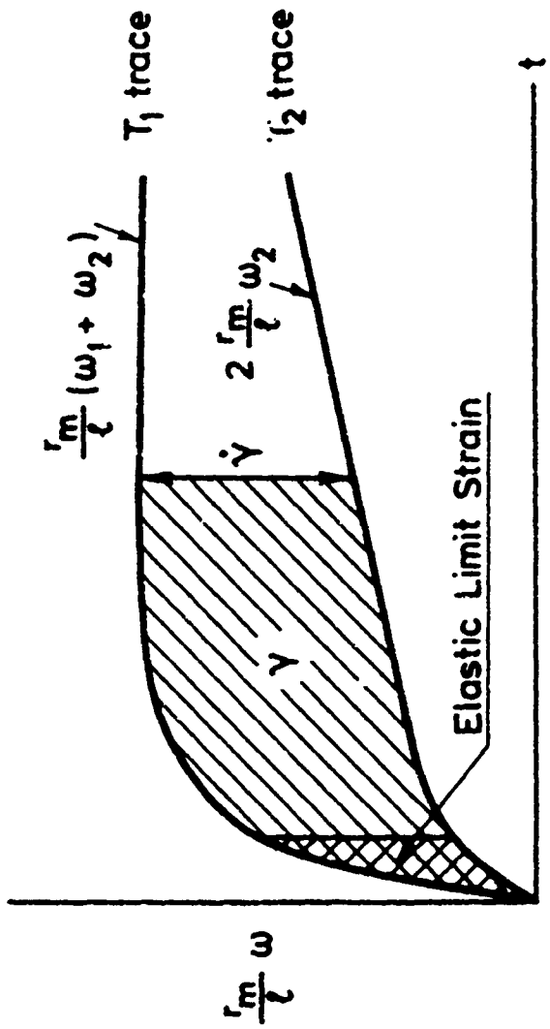

Fig. 5.1 Illustrating calculation of strain and strain rate

(a) $t_k = 0.01881$ in. $r_m = 0.1972$ in.
$\ell = 0.0488$ in. $\dot{\gamma} = 2700\ \text{sec}^{-1}$

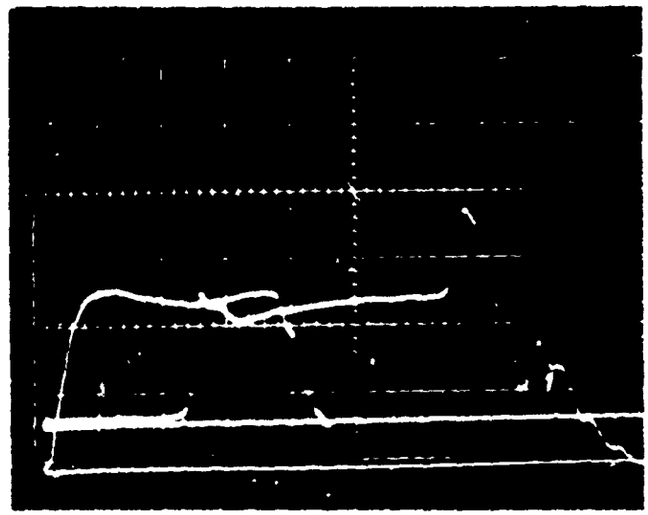

(b) $t_k = 0.01885$ in. $r_m = 0.199$ in.
$\ell = 0.051$ in. $\dot{\gamma} = 1300\ \text{sec}^{-1}$

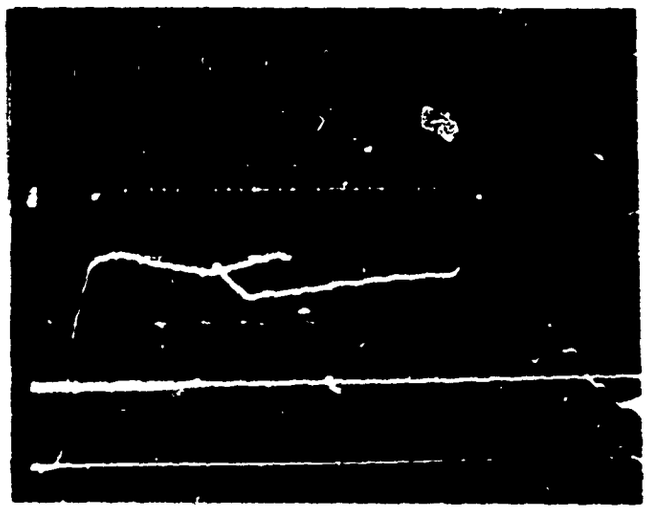

Fig. 6.1.1 Typical oscillograms for EN2A mild steel

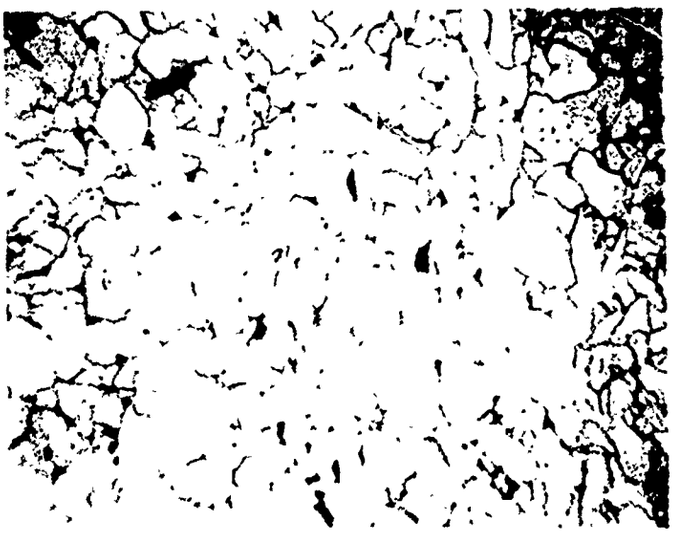

Fig. 6.1.2 Microstructure of EN2A mild steel, X113, grain density 689 gr/mm^2

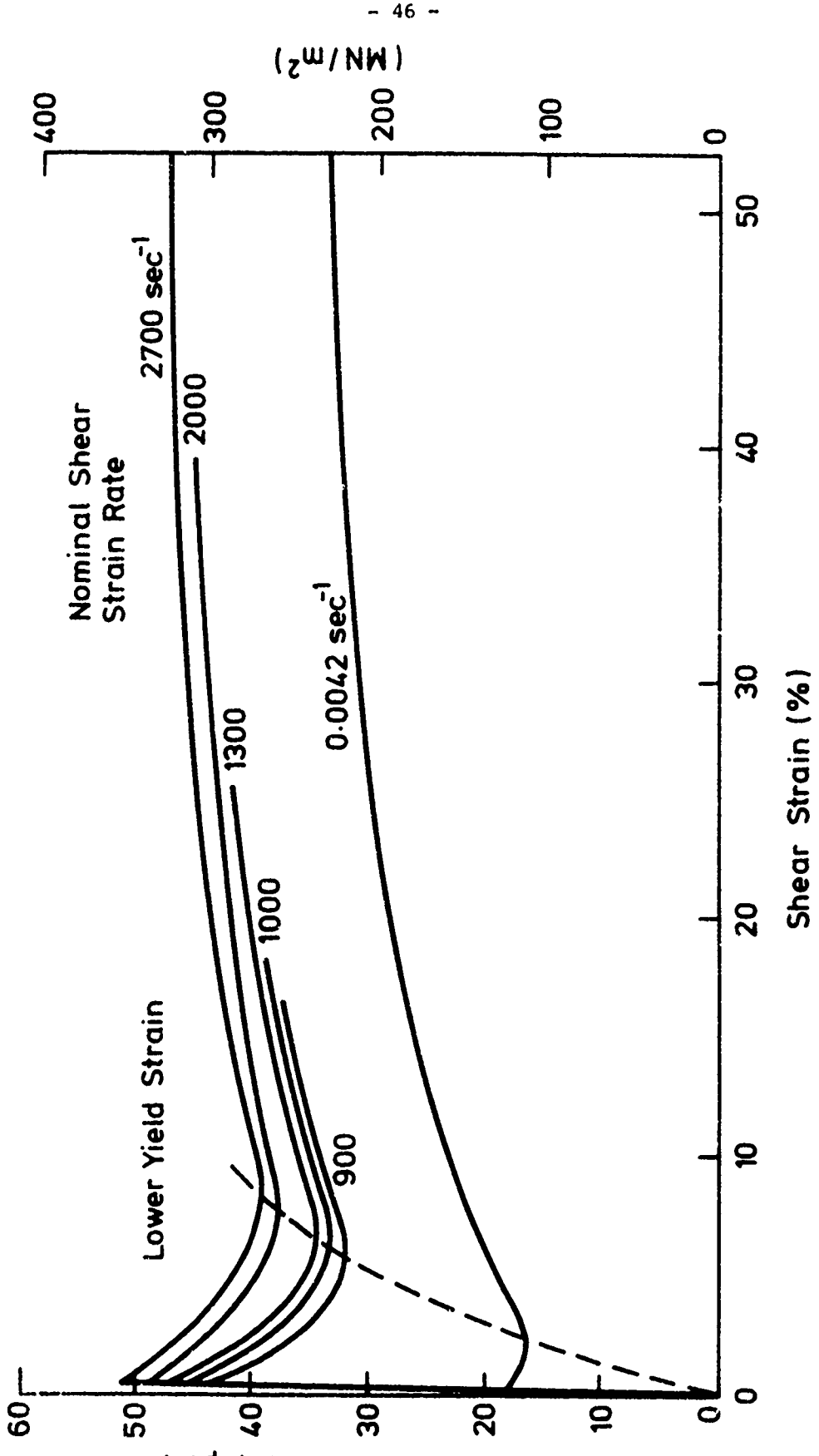

Fig. 6.1.3 (τ,γ) curves for EN2A mild steel

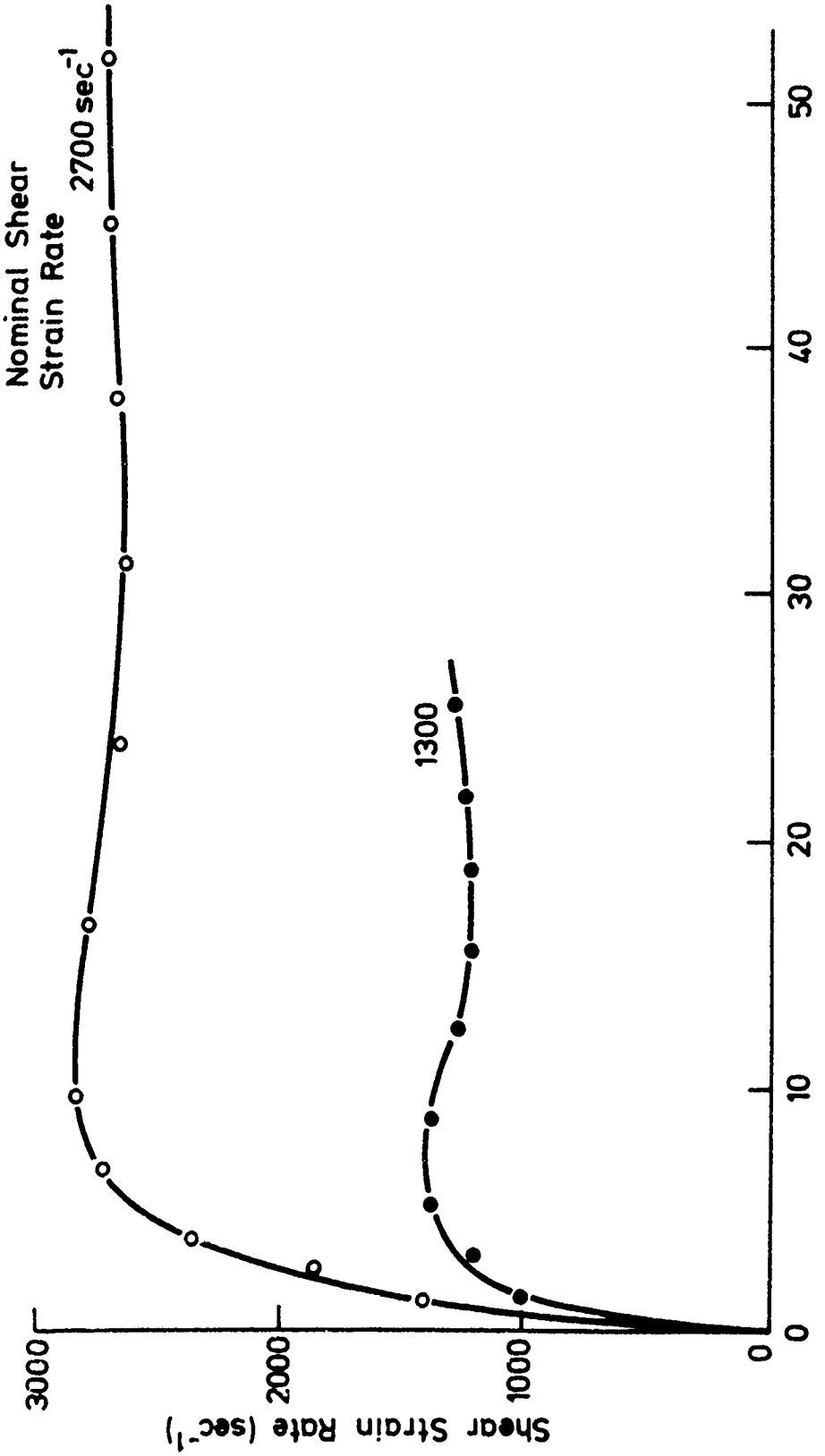

Fig. 6.1.4 $(\dot{\gamma},\gamma)$ curves for EN2A mild steel

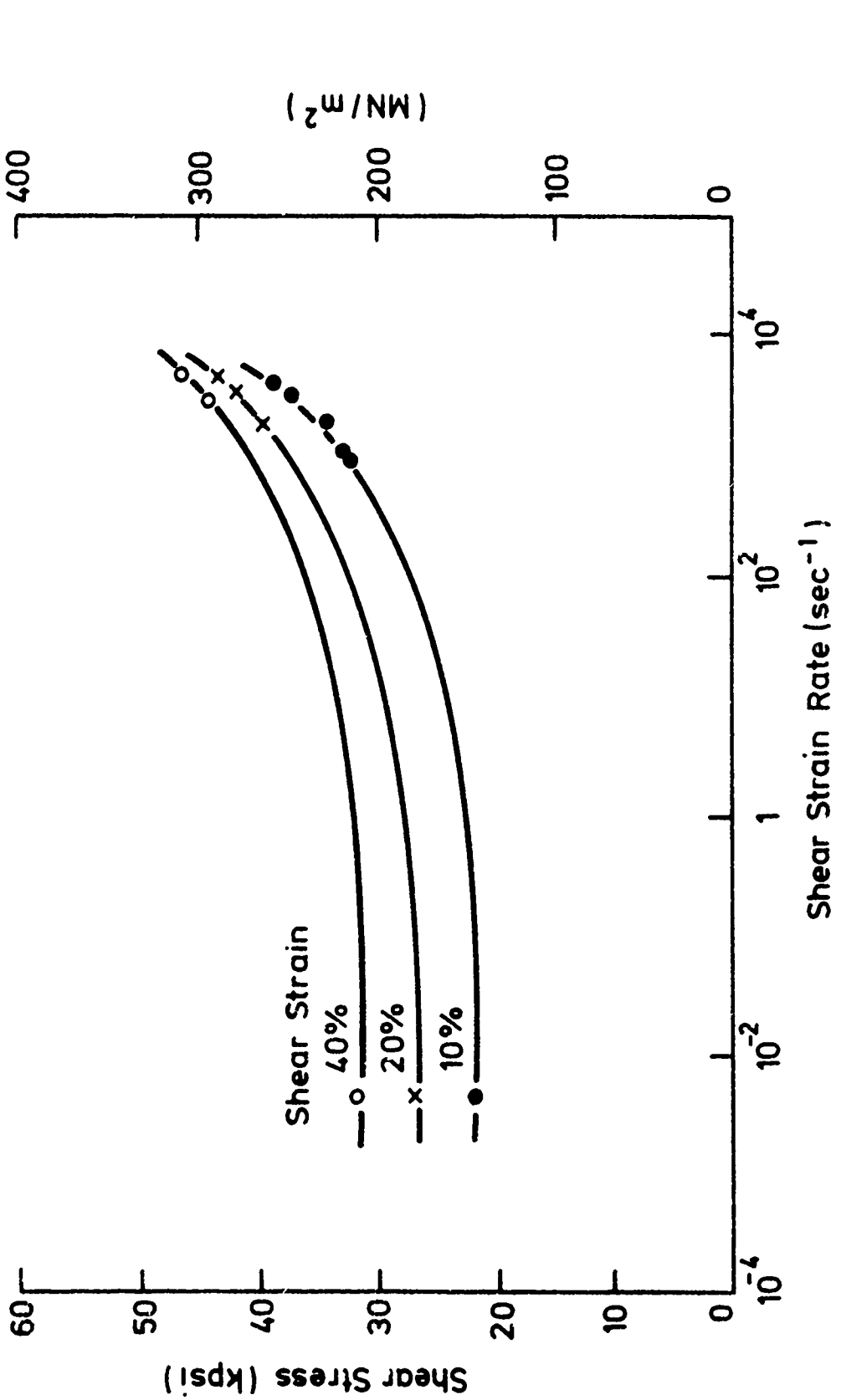

Fig. 6.1.5 (·, log ·) curves for EN2A mild steel

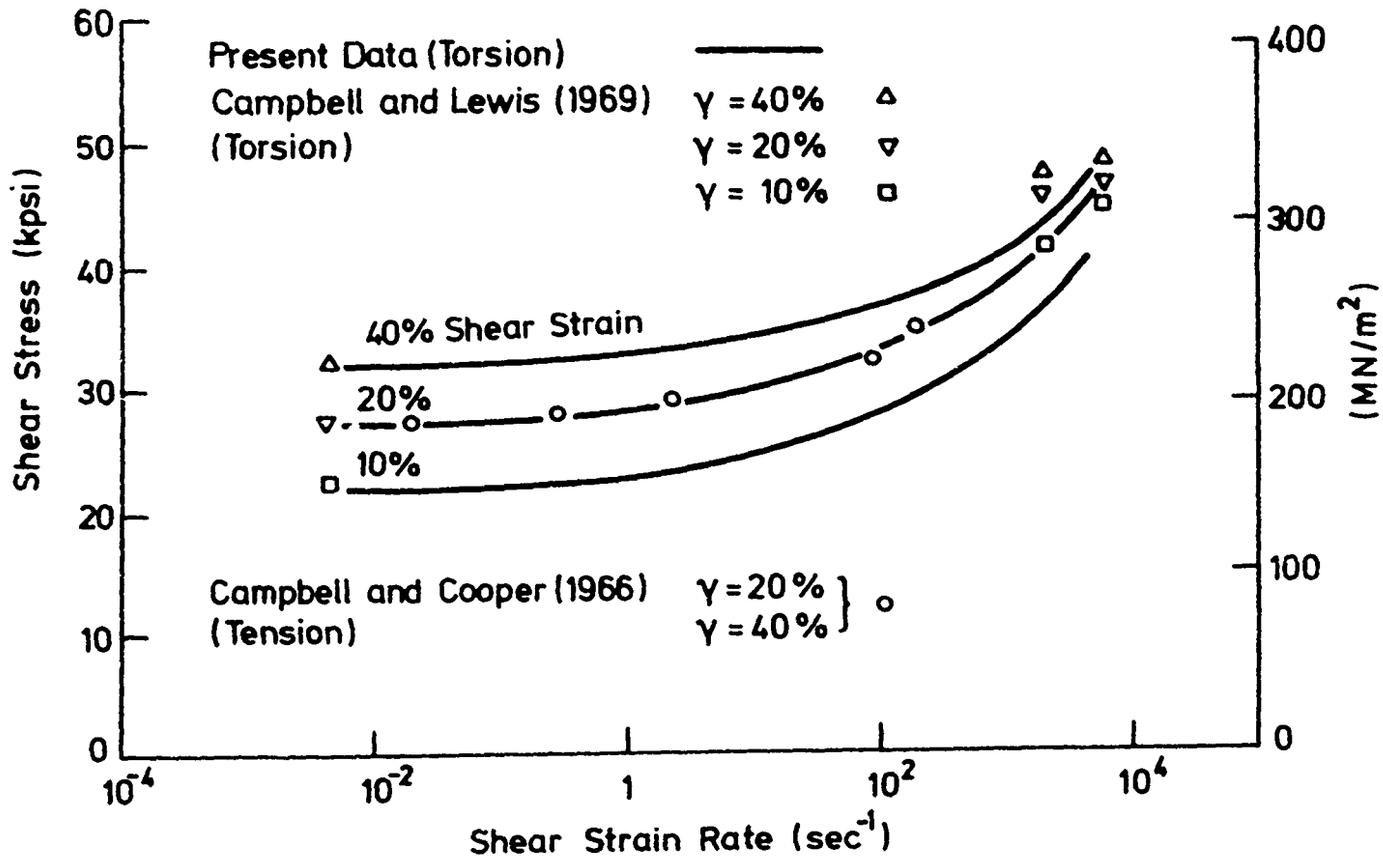

Fig. 6.1.6 Flow stress comparison with earlier work on steels

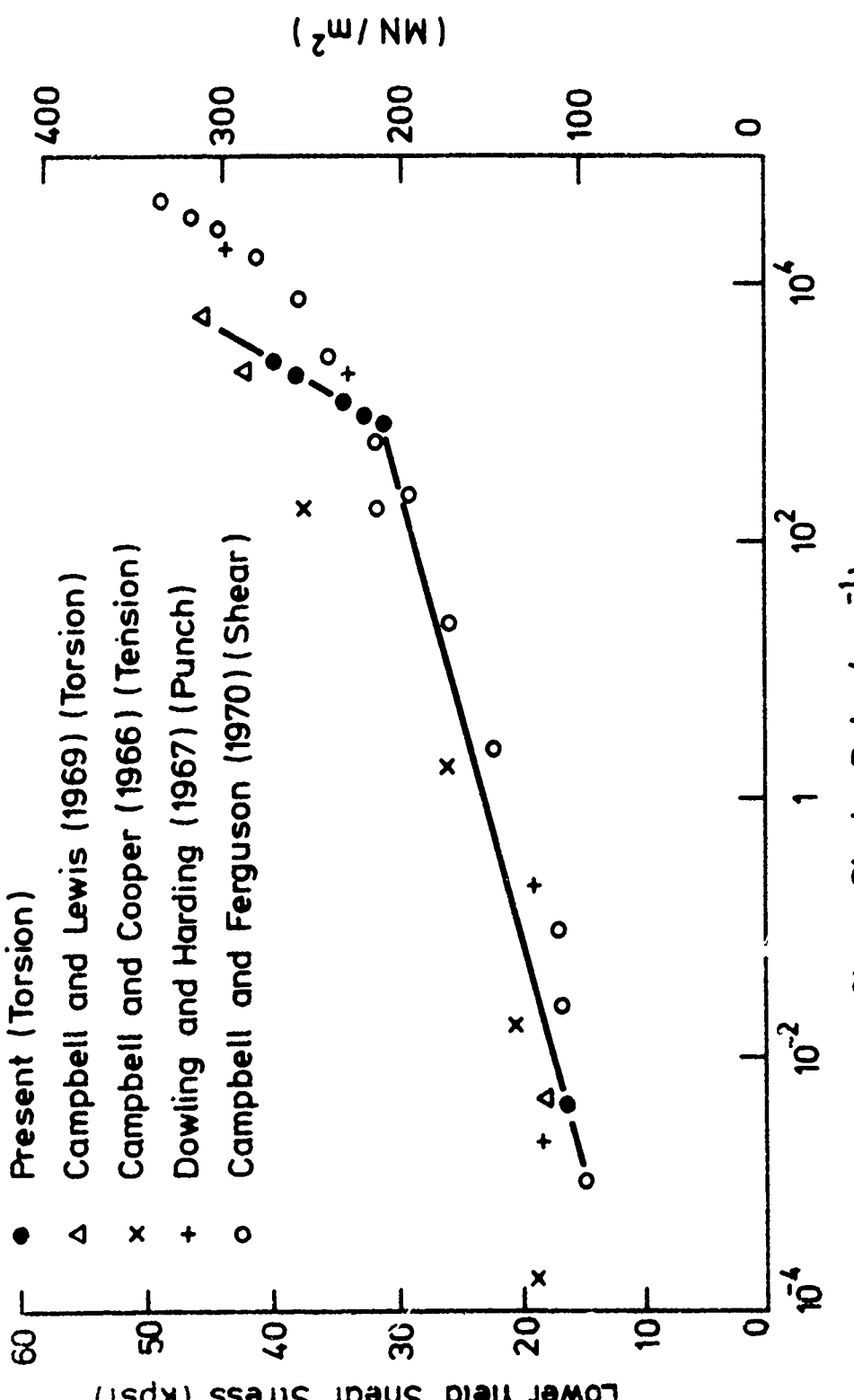

Fig. 6.1.7 Lower yield stress comparison (mild steel)

(a) $t_k = 0.0208$ in. $r_m = 0.1972$ in.
$\ell = 0.050$ in. $\dot{\gamma} = 1500\ sec^{-1}$

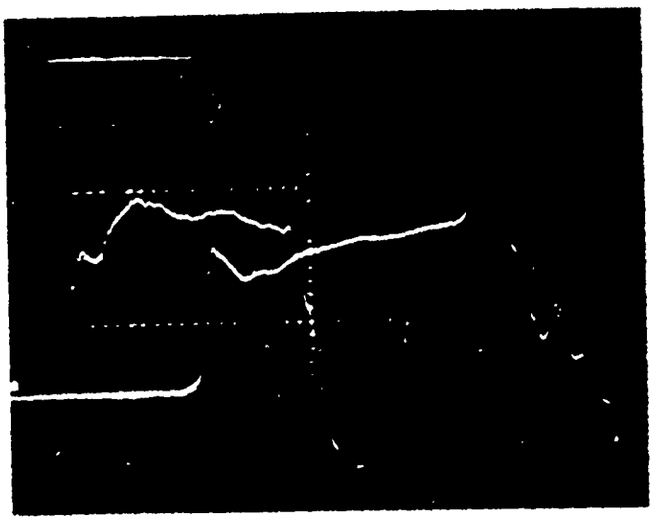

(b) $t_k = 0.01847$ in. $r_m = 0.1977$ in.
$\ell = 0.0471$ in. $\dot{\gamma} = 1200\ sec^{-1}$

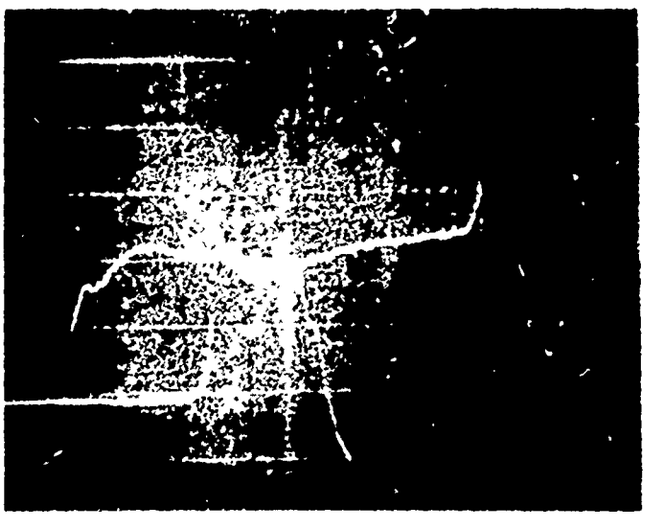

Fig. 6.2.1 Typical oscillograms for EN2D mild steel

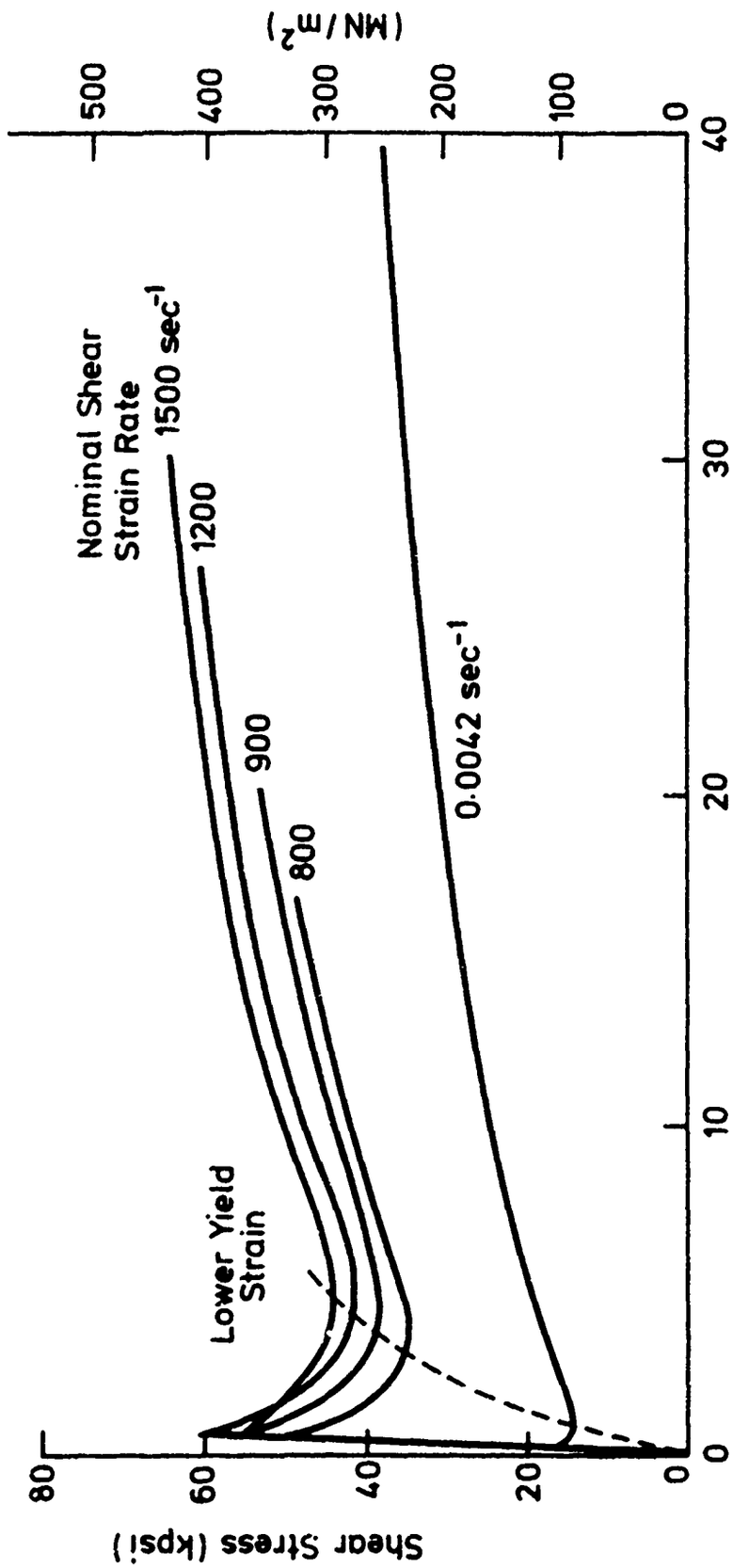

Fig. 6.2.2 (...) curves for EN2D mild steel

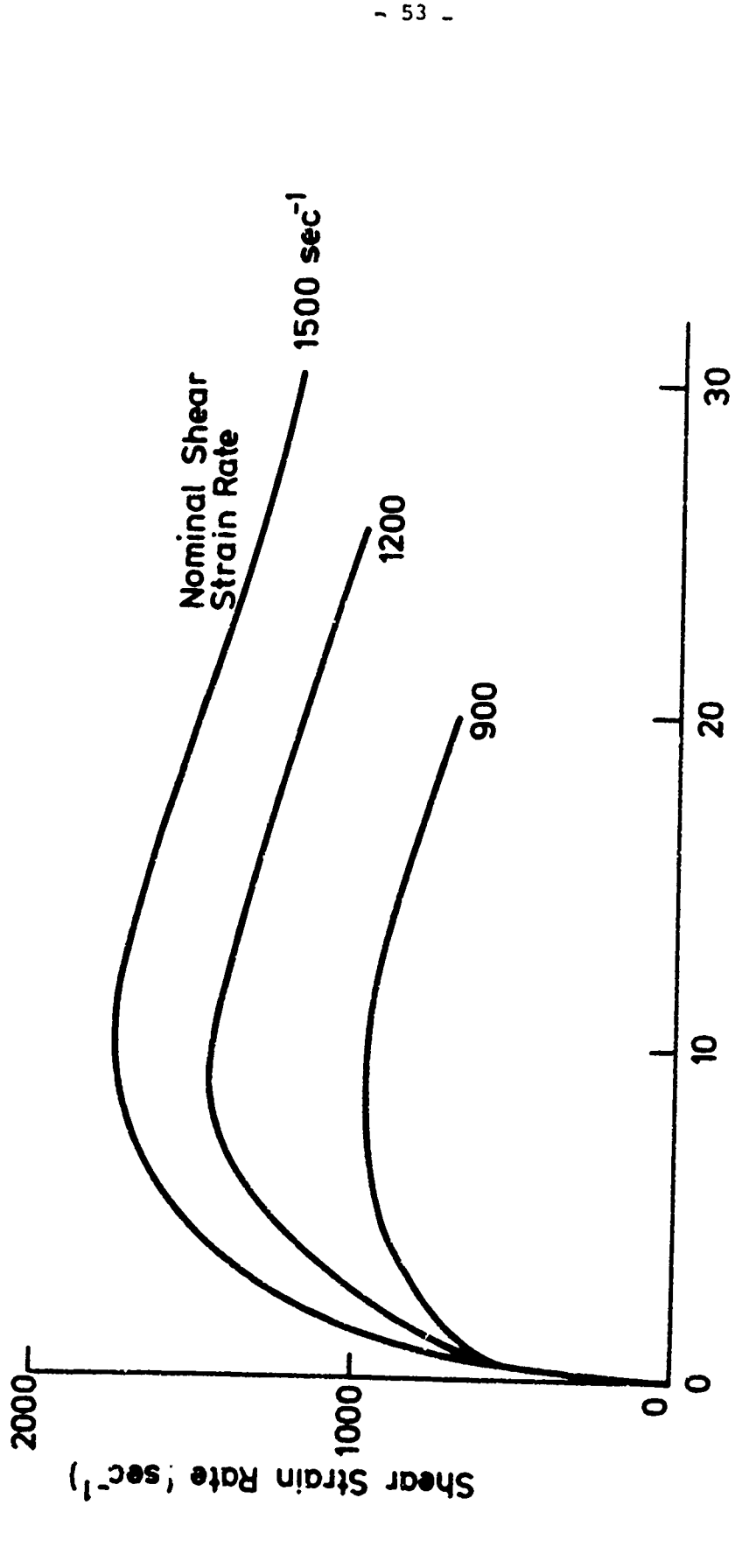

Fig. 6.2.3 $(\dot{\gamma}, \gamma)$ curves for EN2D mild steel

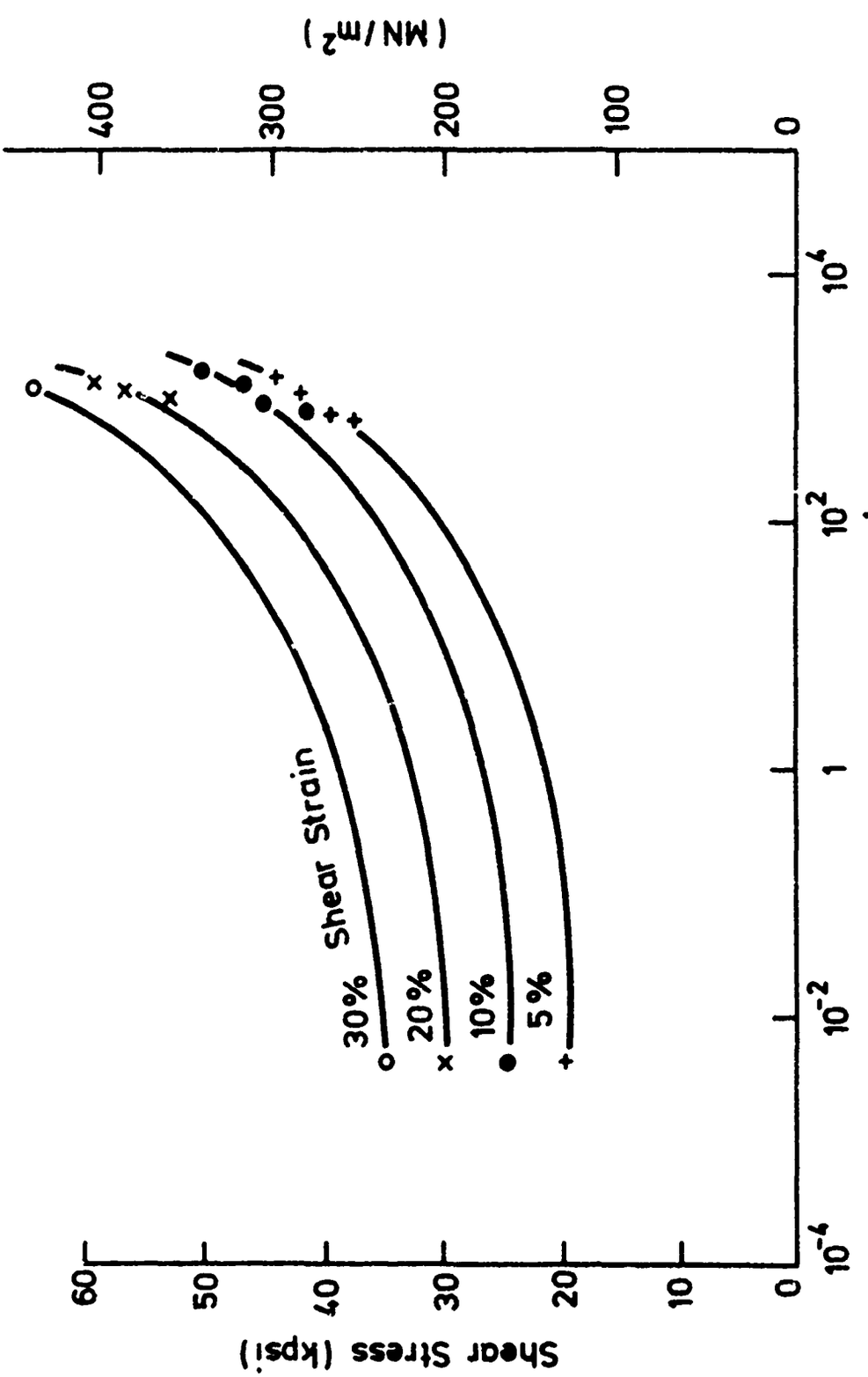

Fig. 6.2.4 (·, log $\dot{\gamma}$) curves for EN2D mild steel

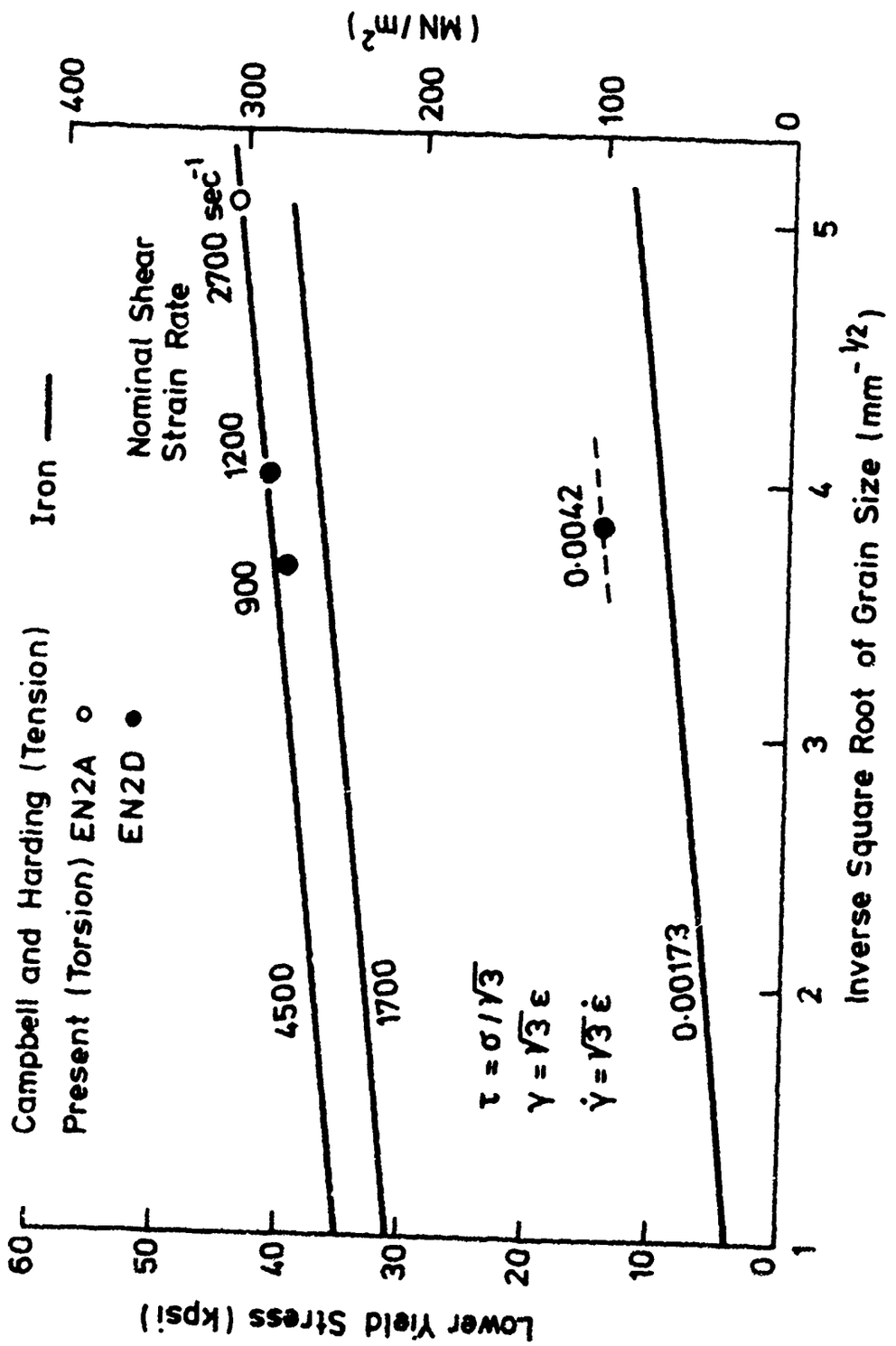

Fig. 6.2.5 Lower yield stress variation with grain size

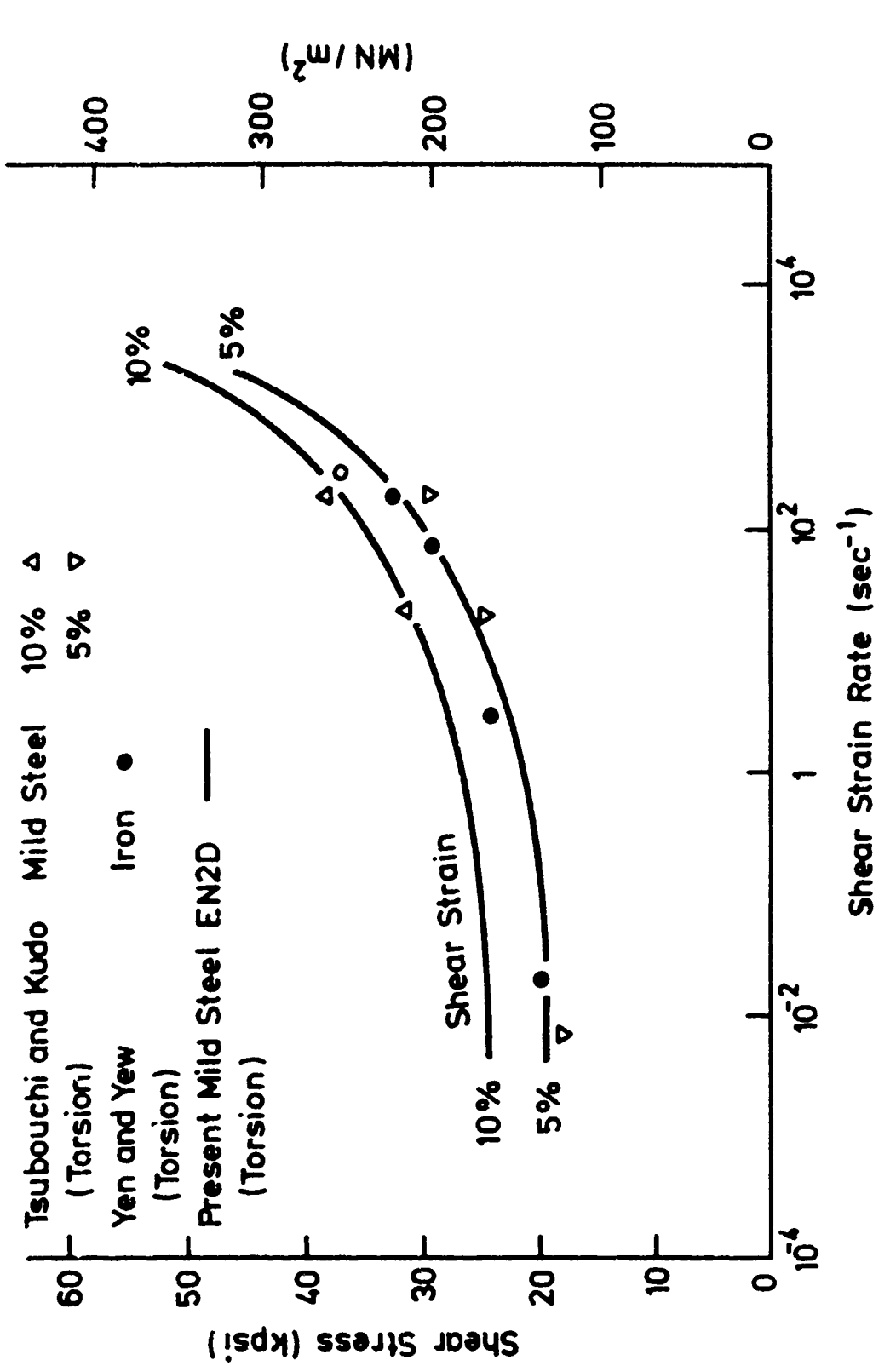

Fig. 6.2.6 (τ, log $\dot{\gamma}$) curves for steels

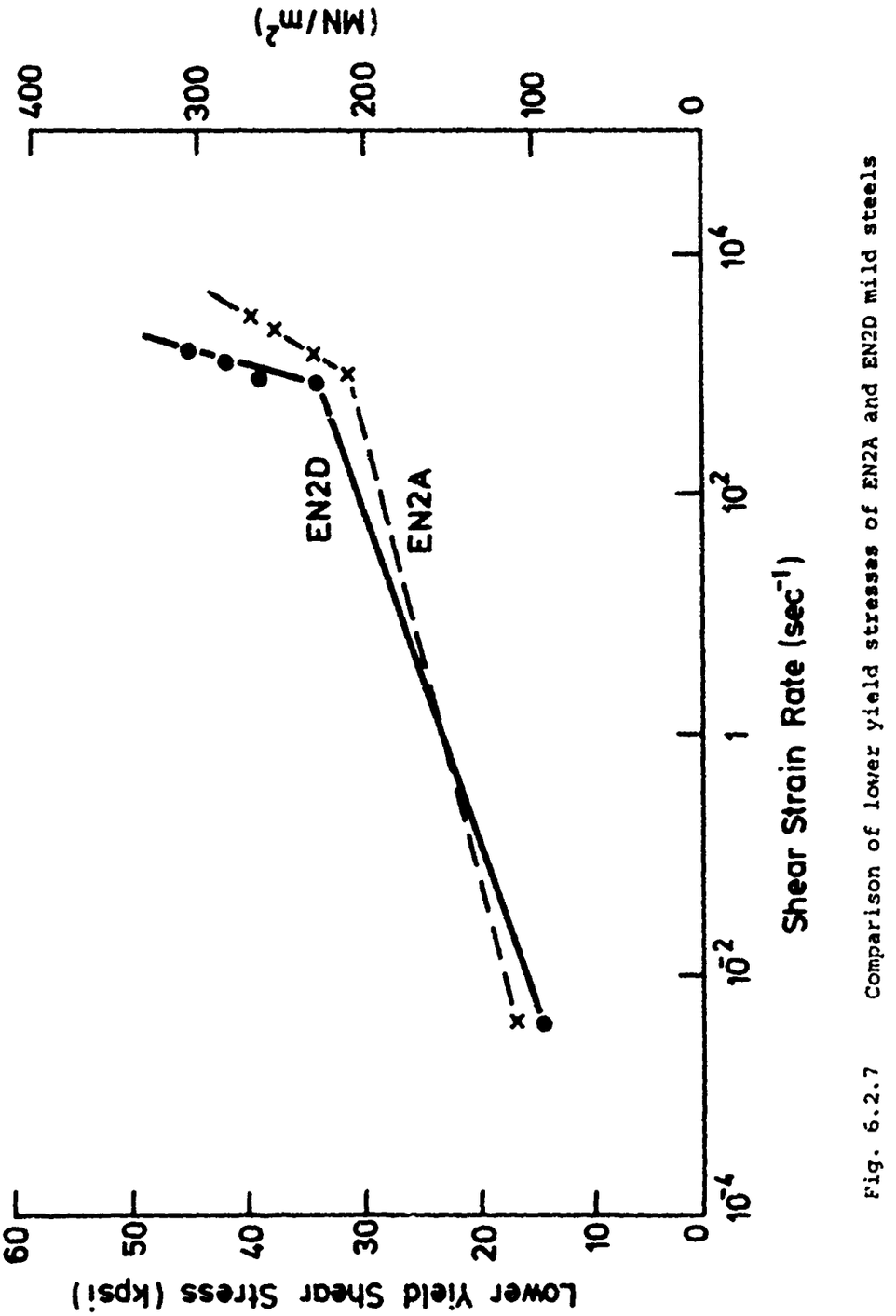

Fig. 6.2.7 Comparison of lower yield stresses of EN2A and EN2D mild steels

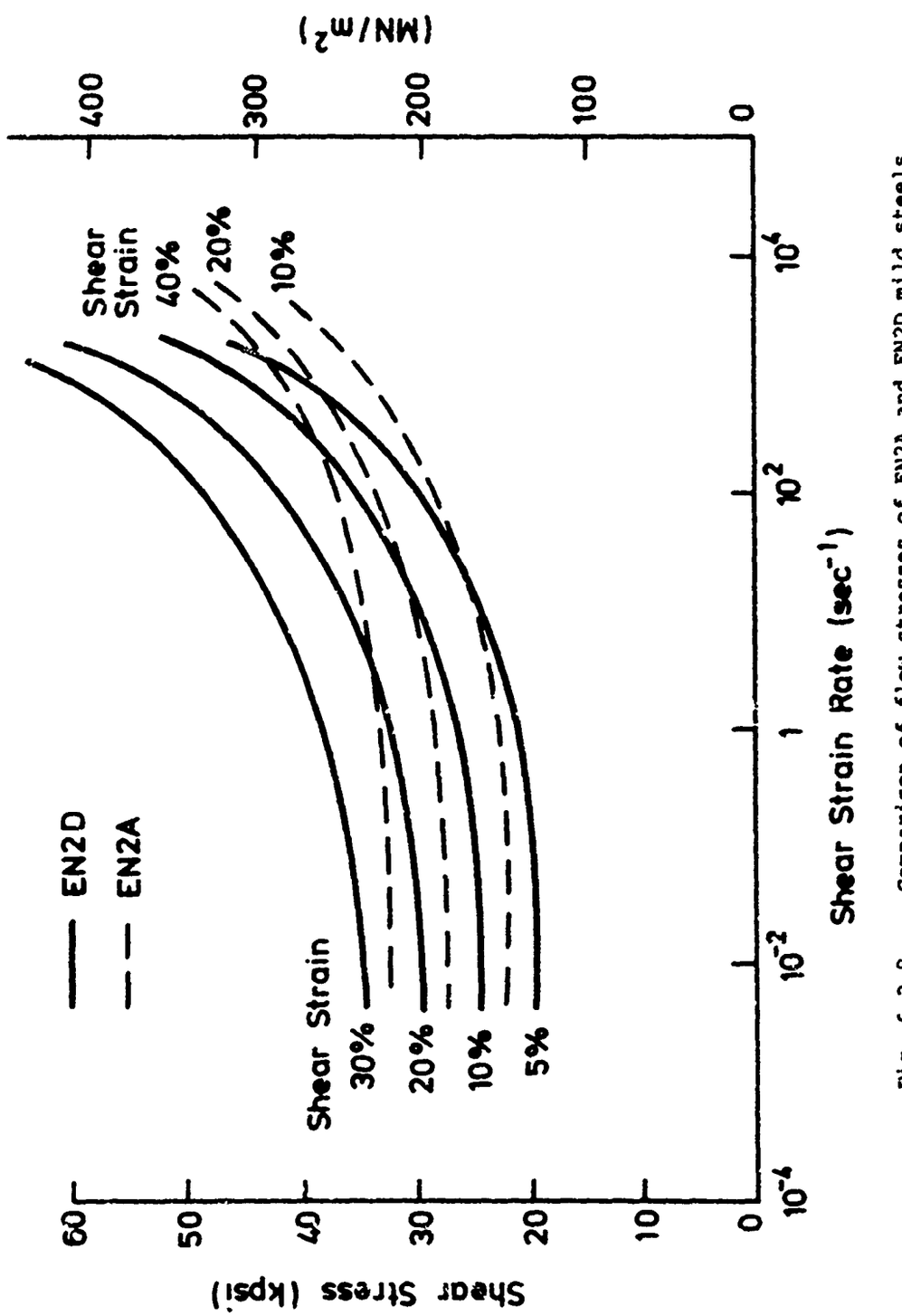

Fig. 6.2.8 Comparison of flow stresses of EN2A and EN2D mild steels

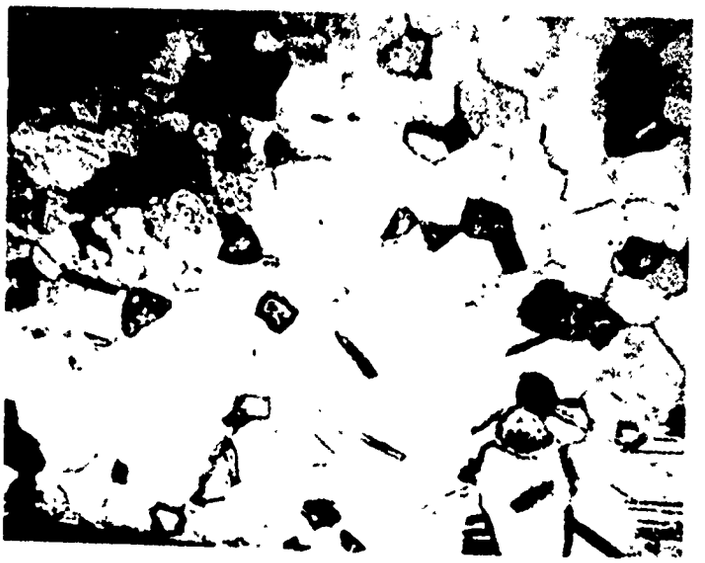

Fig. 6.3.1 Microstructure of titanium, X113, grain density 340 gr/mm^2

(a) $t_k = 0.0200$ in. $r_m = 0.201$ in.

$\ell = 0.0494$ in. $\dot{\gamma} = 1250 \ \text{sec}^{-1}$

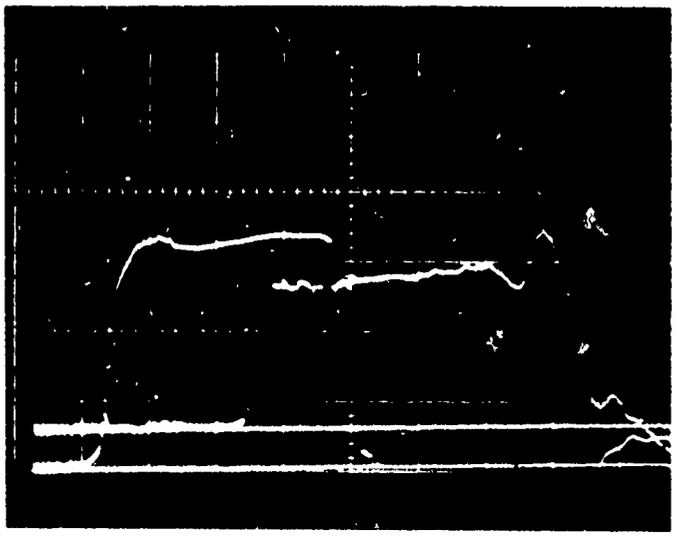

(b) $t_k = 0.02087$ in. $r_m = 0.198$ in.

$\ell = 0.0493$ in. $\dot{\gamma} = 2000 \ \text{sec}^{-1}$

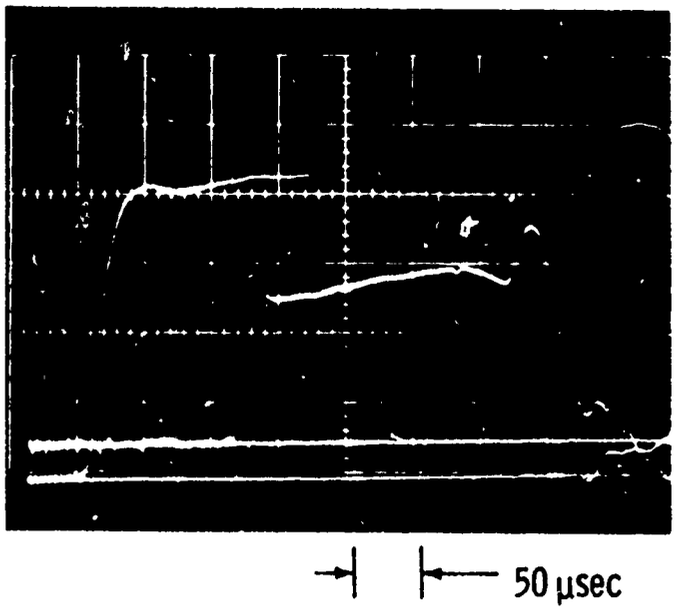

Fig. 6.3.2 Typical oscillograms for titanium

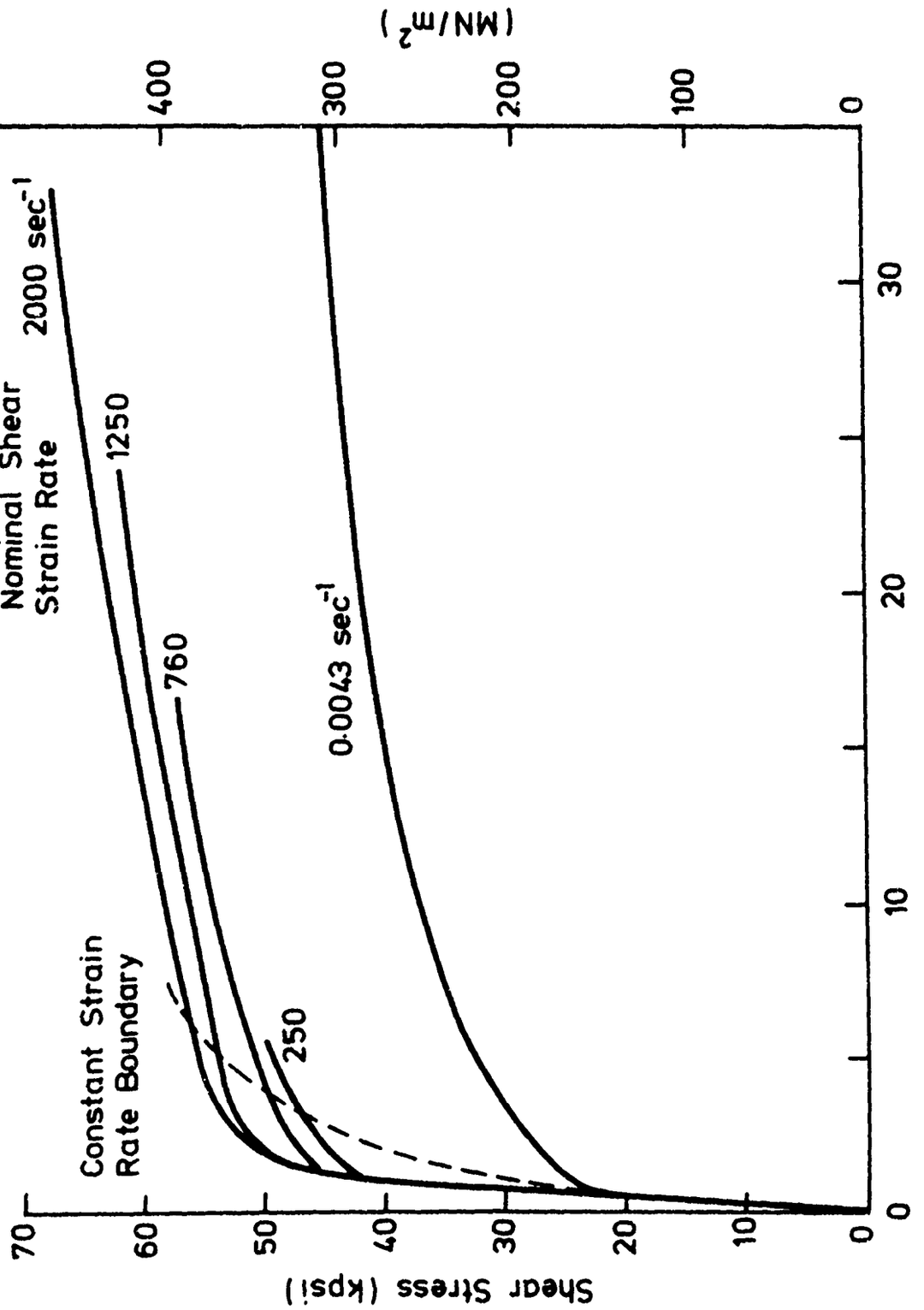

Fig. 6.3.3 (:,:) curves for titanium

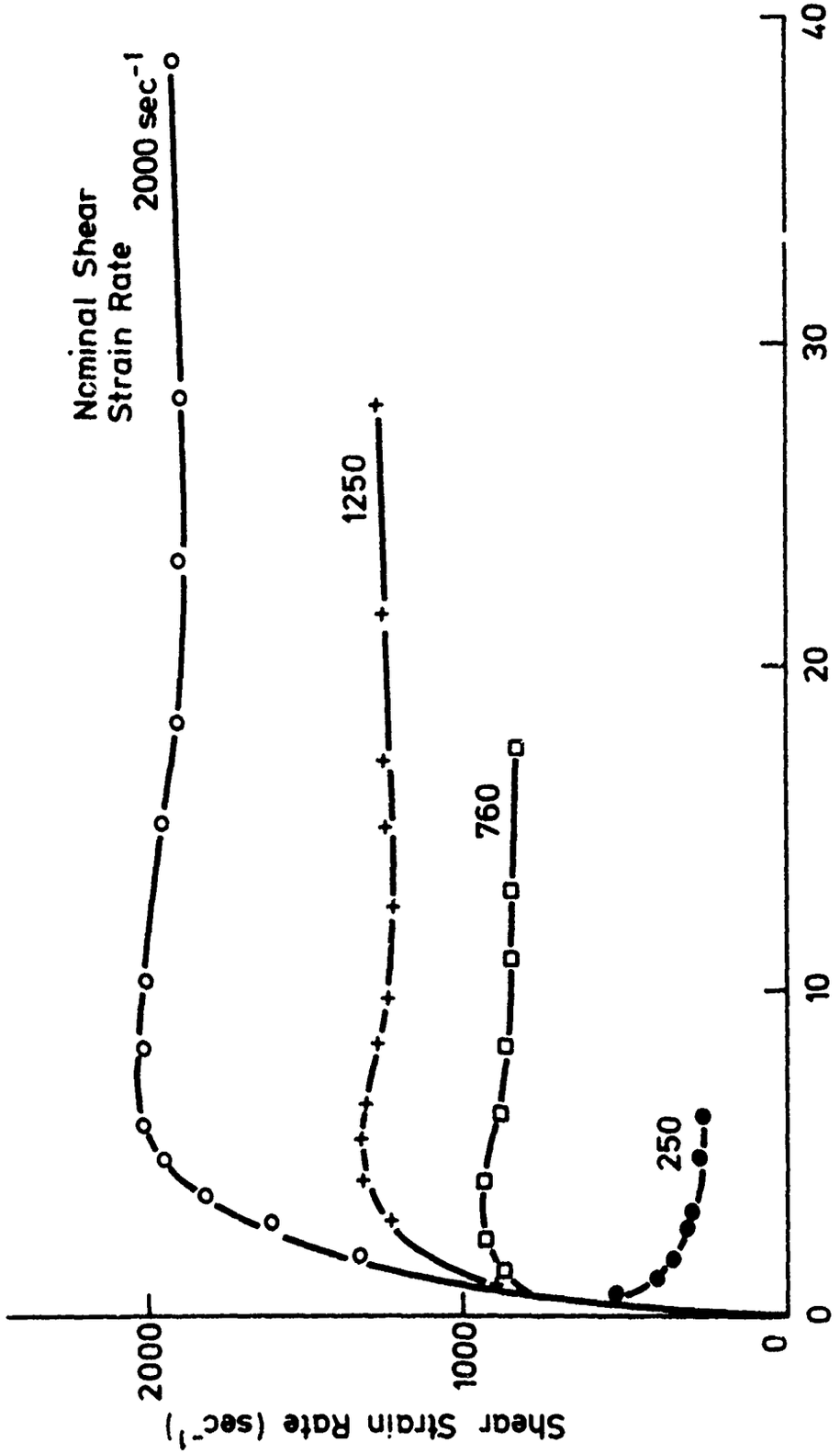

Fig. 6.3.4 $(\gamma, \dot{\gamma})$ curves for titanium

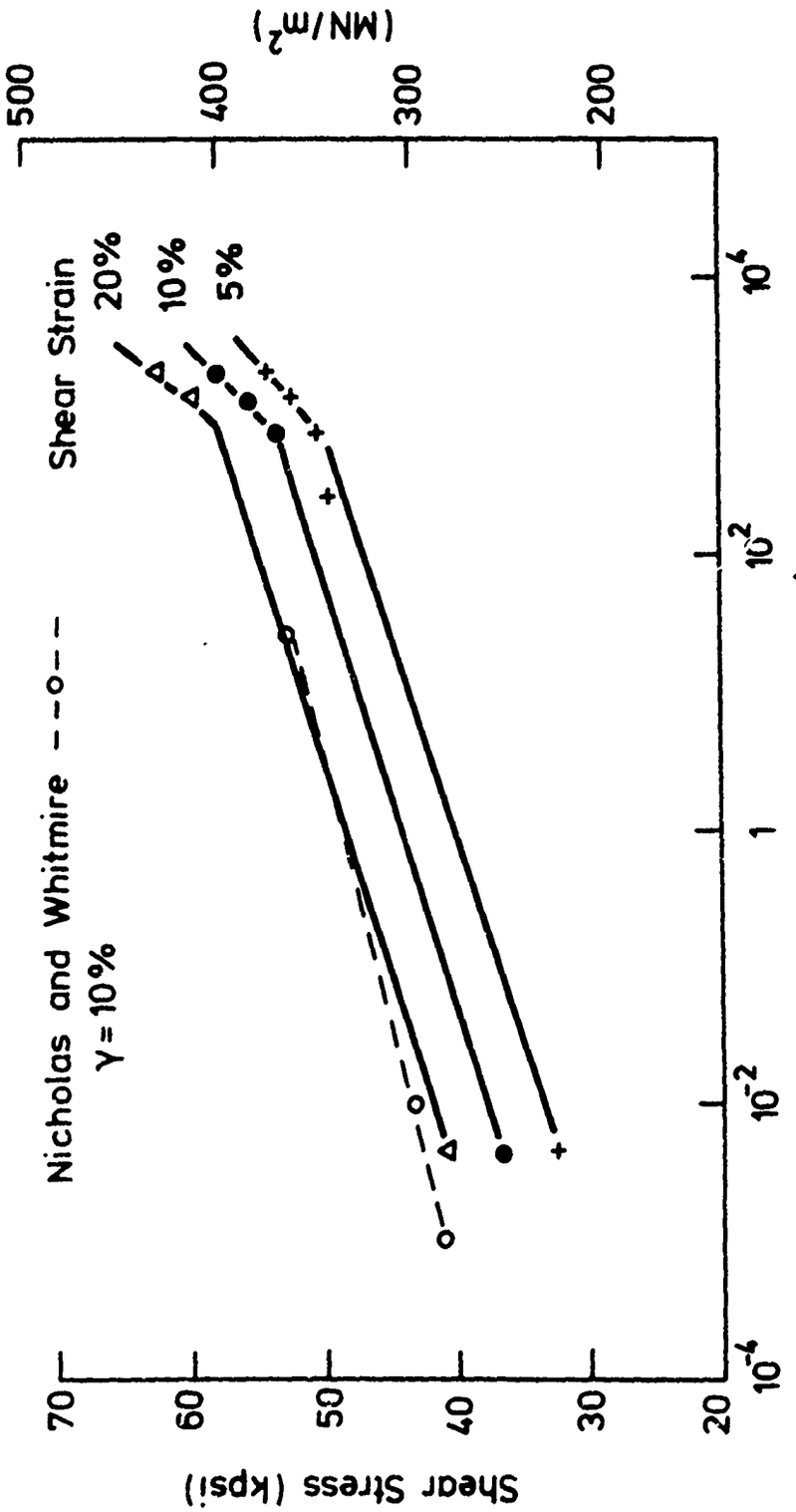

Fig. 6.3.5 (τ, log $\dot{\gamma}$) curves for titanium

(a) $t_k = 0.0204$ in. $r_m = 0.1976$ in.
$\ell = 0.0504$ in. $\dot{\gamma} = 600 \quad sec^{-1}$

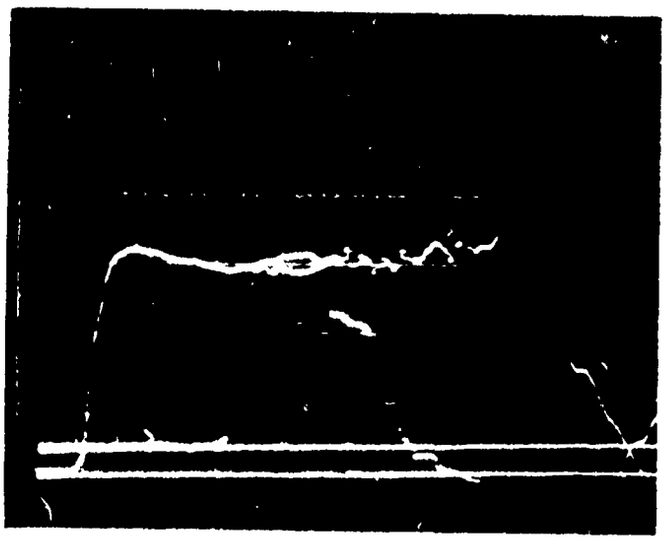

(b) $t_k = 0.01782$ in. $r_m = 0.1976$ in.
$\ell = 0.0523$ in. $\dot{\gamma} = 2100 \quad sec^{-1}$

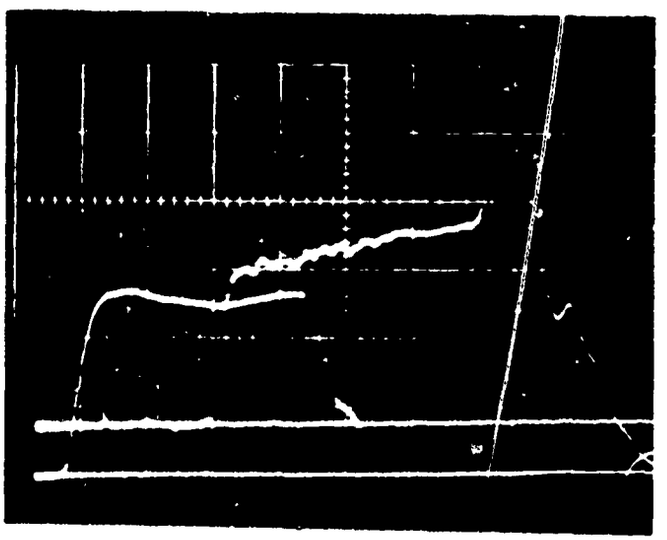

Fig. 6.4.1 Typical oscillograms for stainless steel

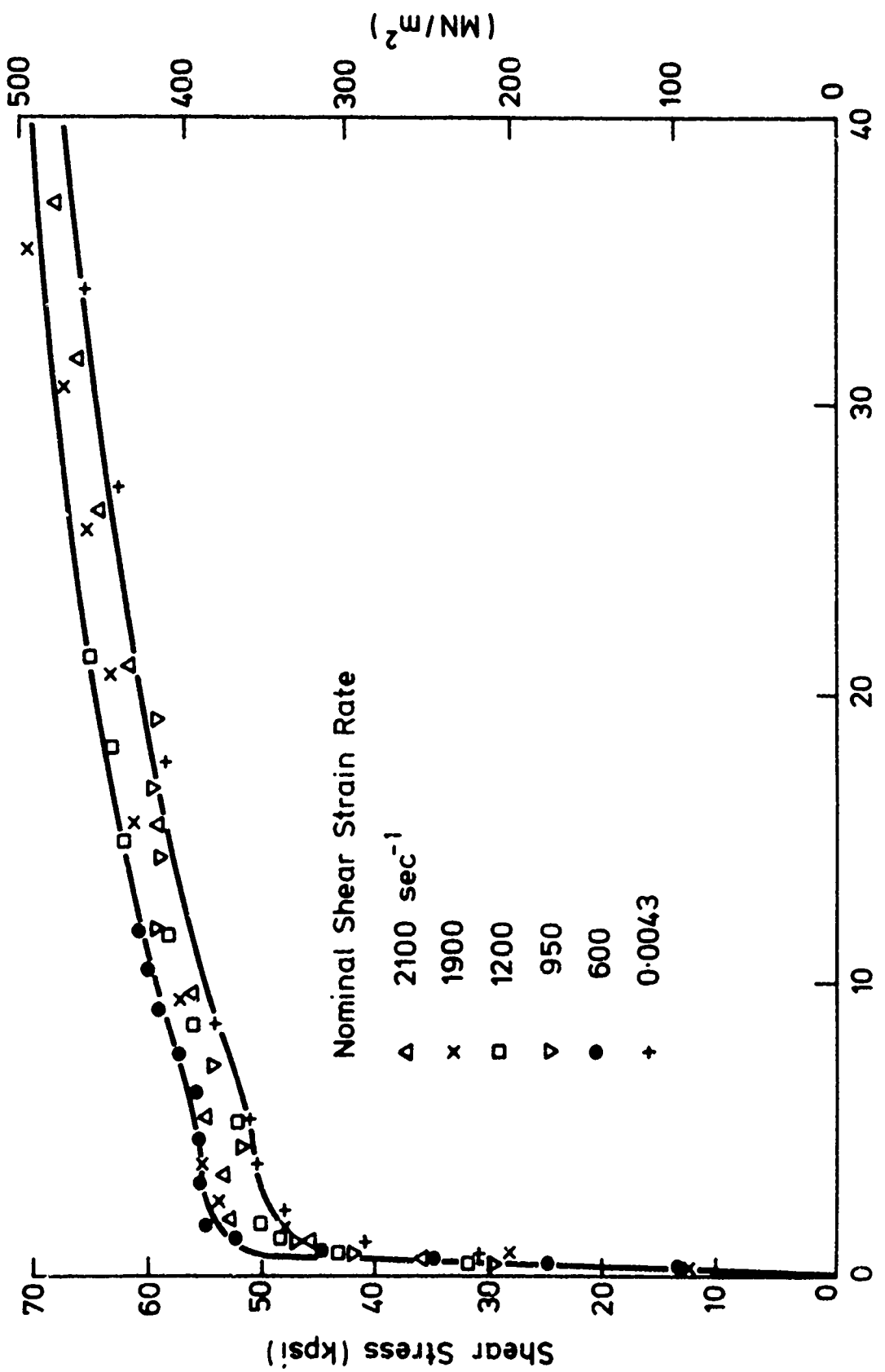

Fig. 6.4.2 (·,·) curves for stainless steel

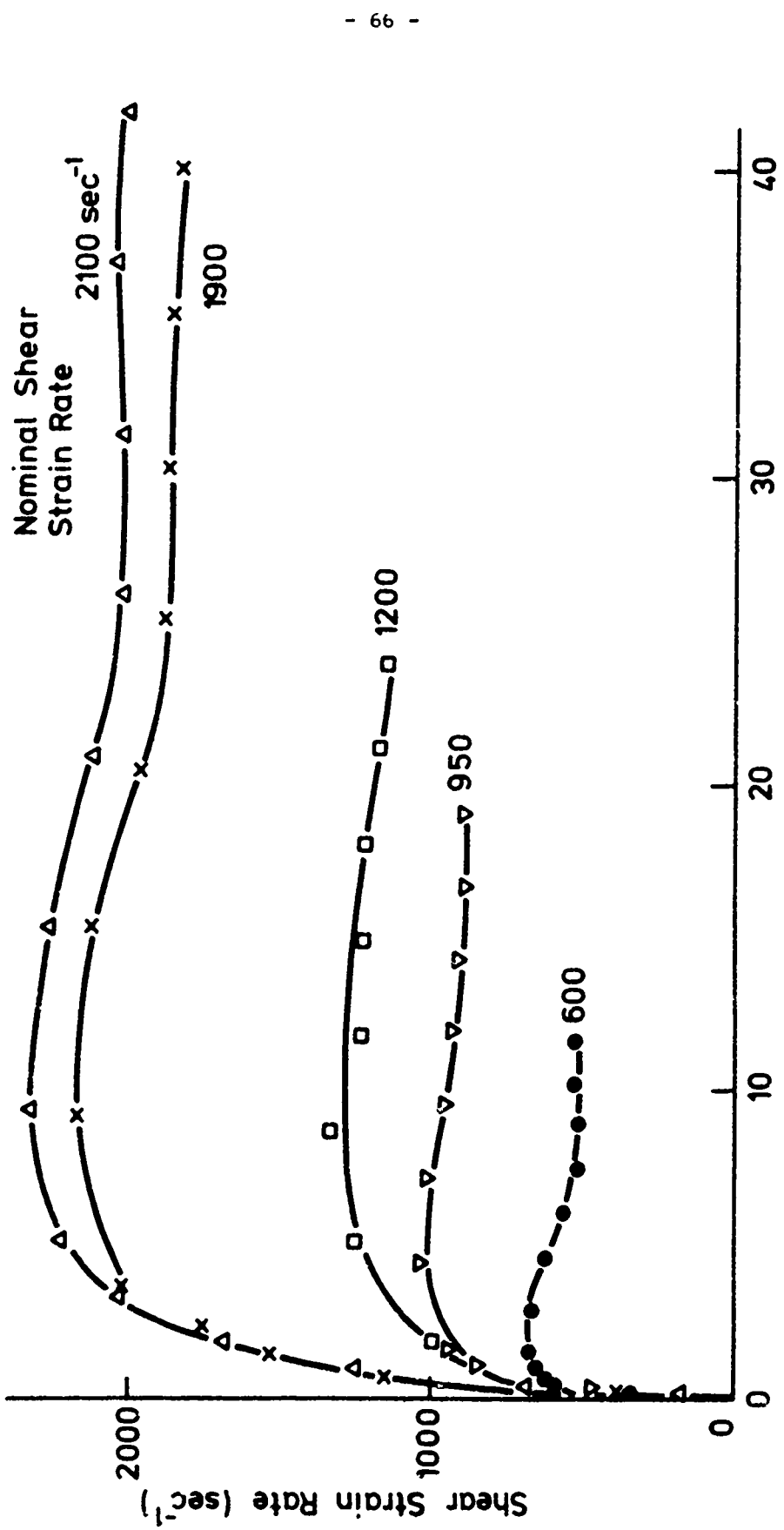

Fig. 6.4.3 $(\gamma, \dot{\gamma})$ curves for stainless steel

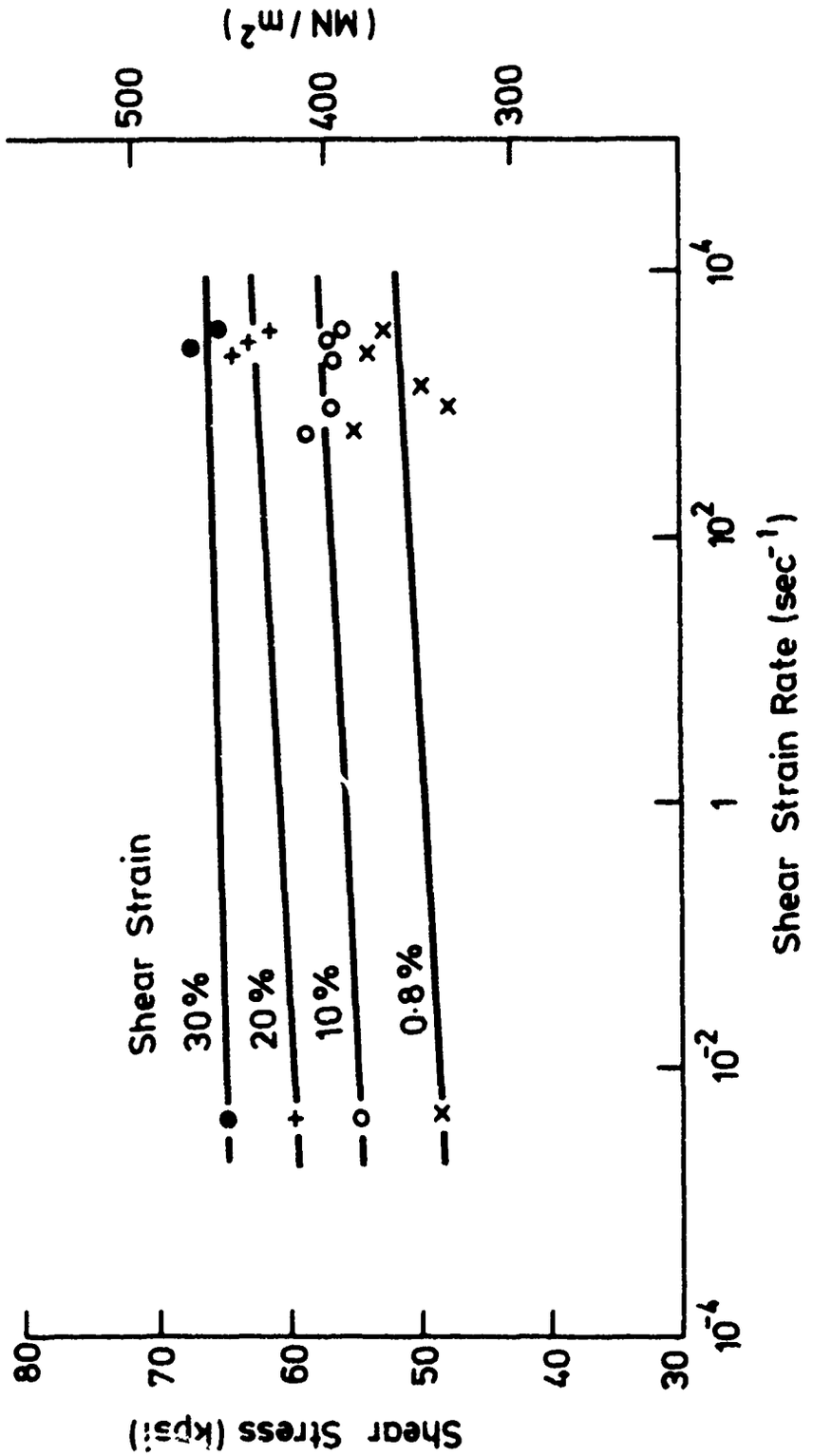

Fig. 6.4.4 (τ, log $\dot{\gamma}$) curves for stainless steel

Fig. 6.5.1 Microstructure of copper, X242, grain density 1320 gr/mm^2

(a) $t_k = 0.0172$ in. $r_m = 0.1972$ in.
$\ell = 0.0463$ in. $\dot{\gamma} = 1125 \quad sec^{-1}$

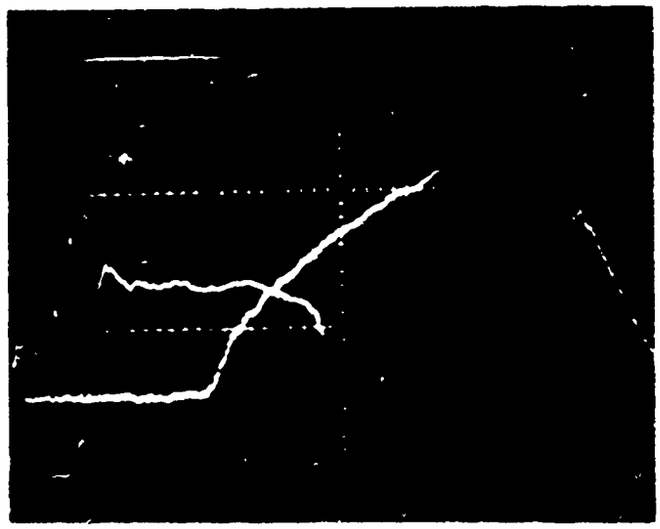

(b) $t_k = 0.01766$ in. $r_m = 0.1968$ in.
$\ell = 0.0480$ in. $\dot{\gamma} = 3000 \quad sec^{-1}$

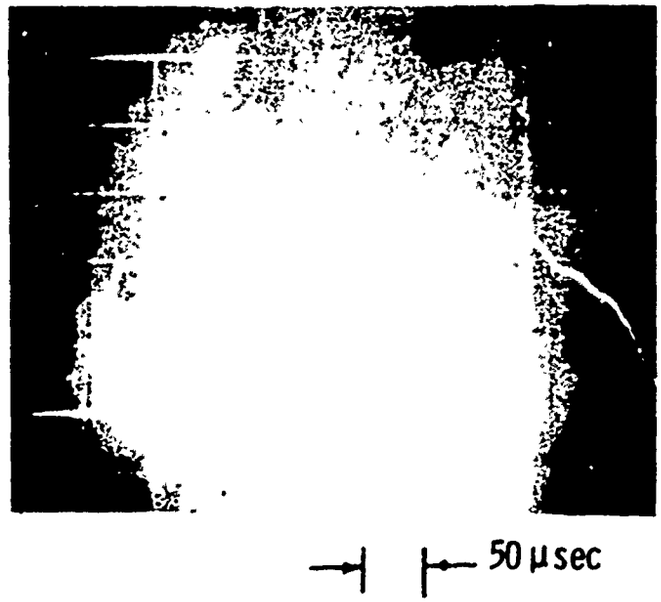

Fig. 6.5.2 Typical oscillograms for copper

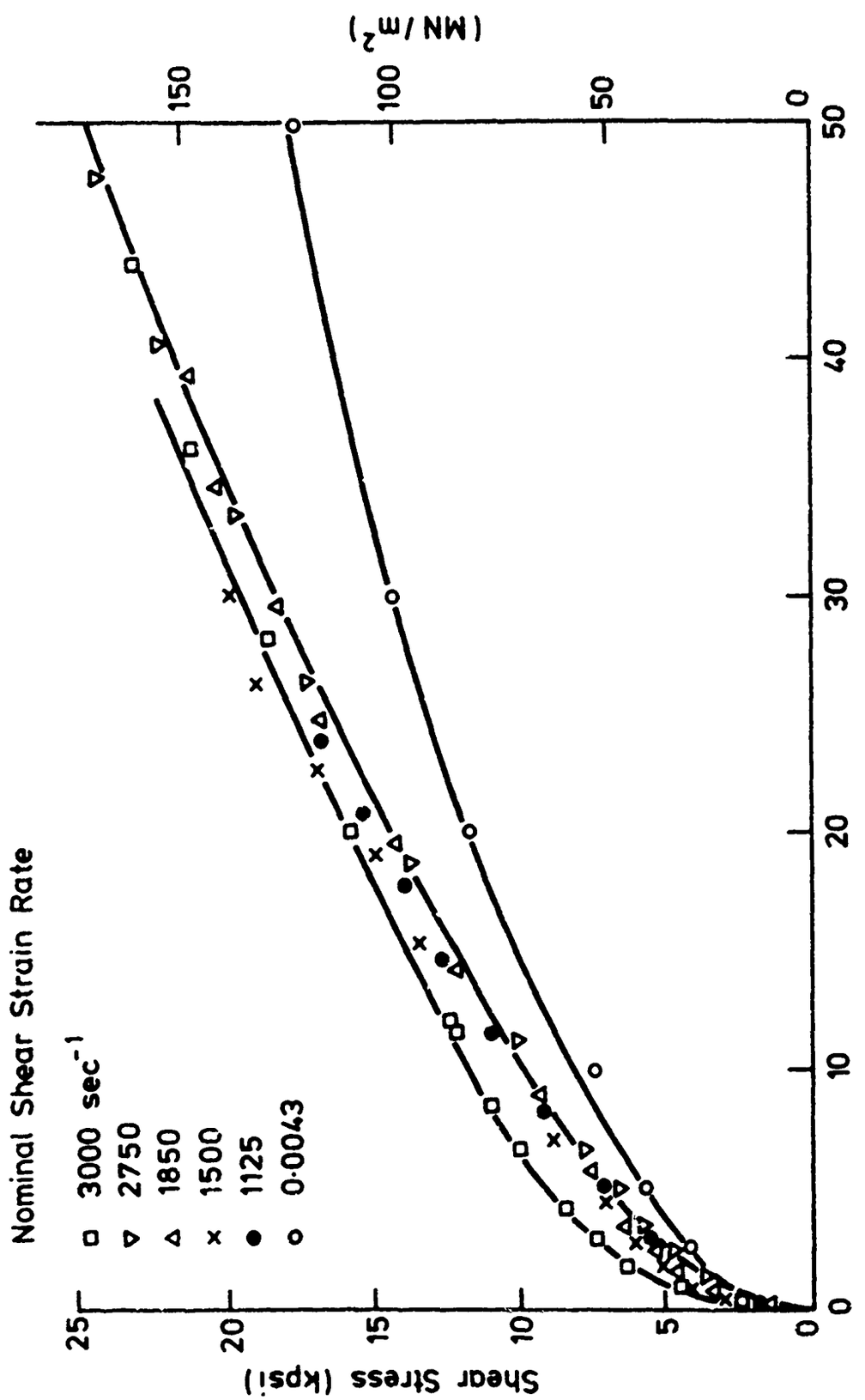

Fig. 6.5.3 (·,·) curves for copper

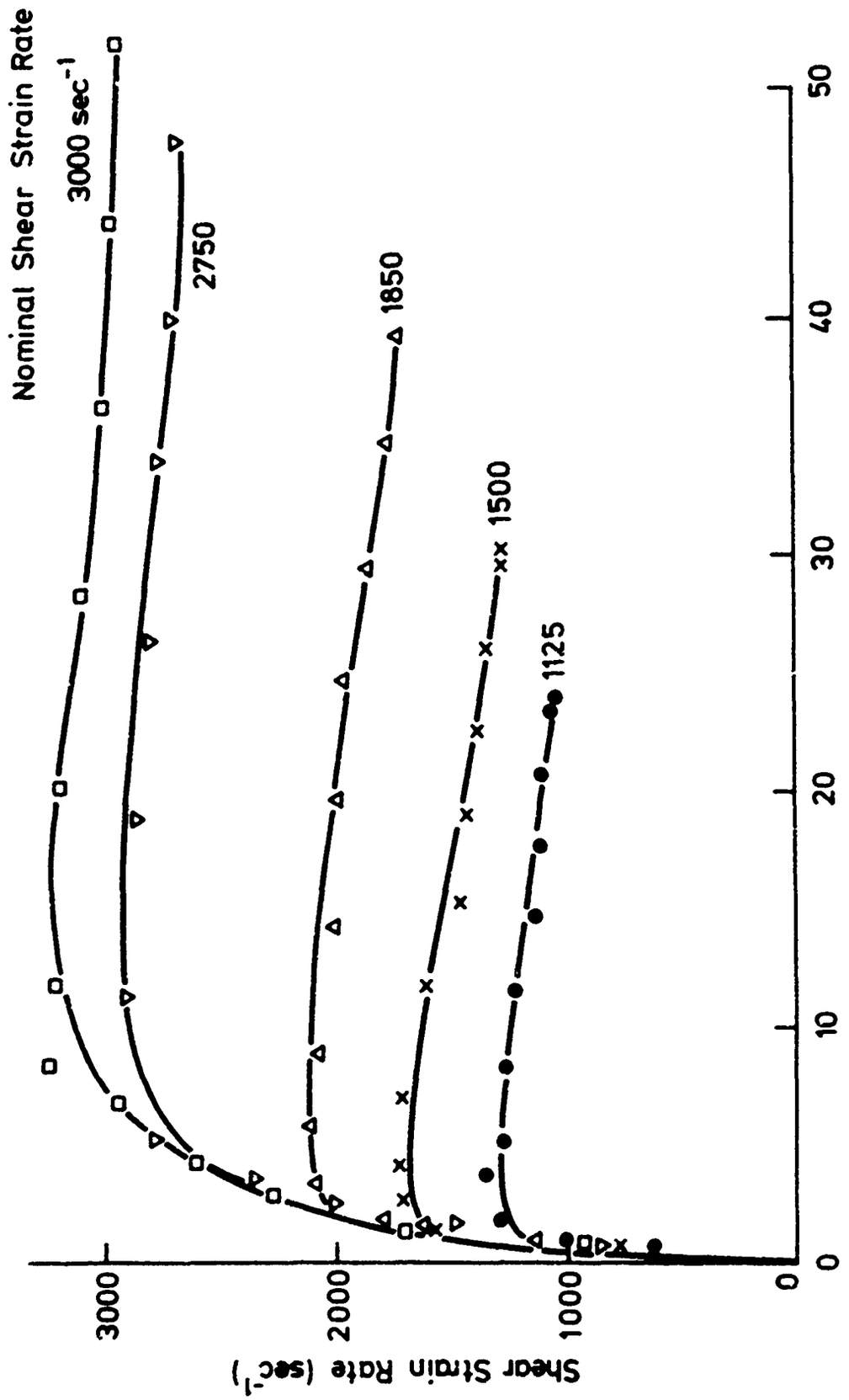

Fig. 6.5.4 $(\tau,\dot{\gamma})$ curves for copper

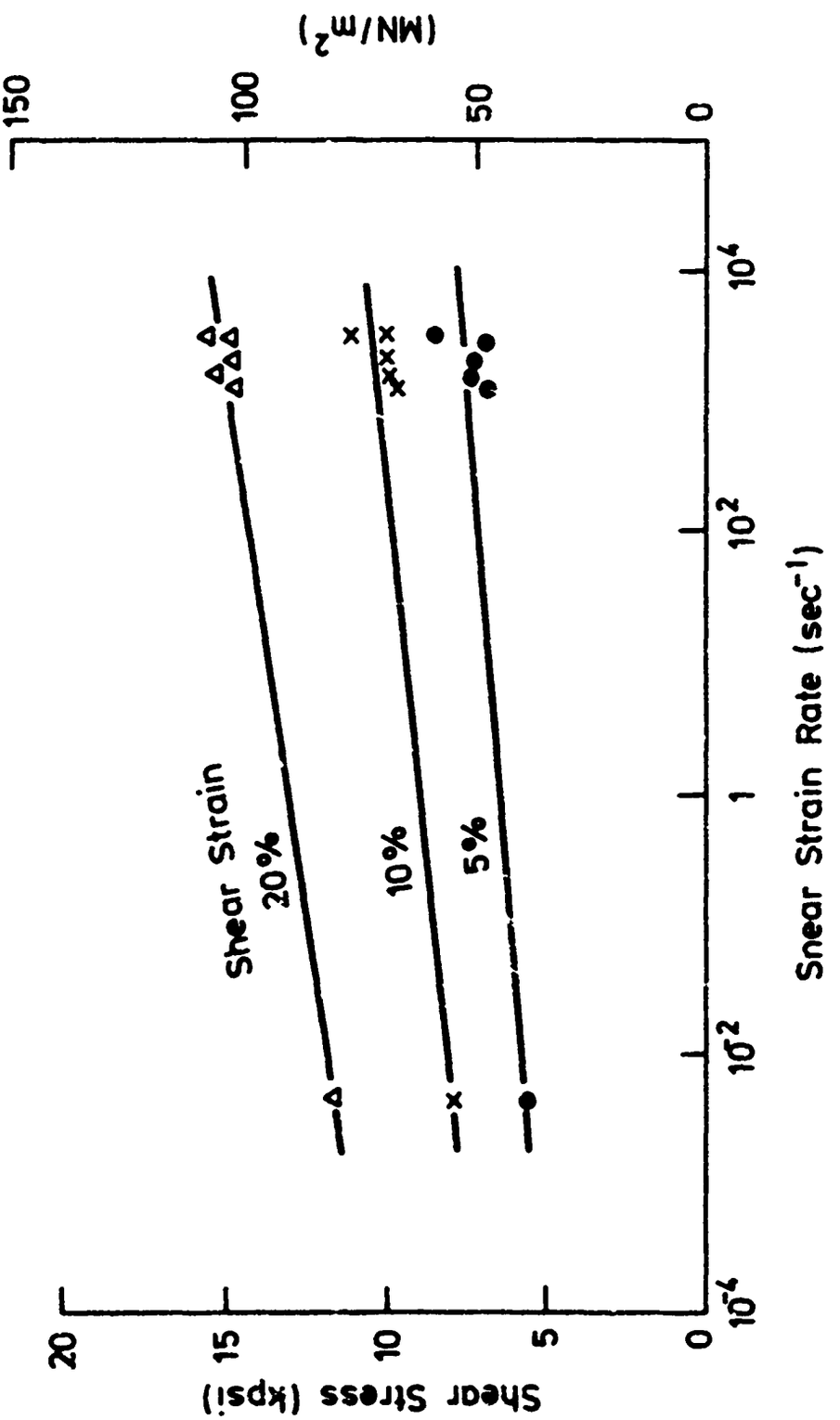

Fig. 6.5.5 (τ, log $\dot{\gamma}$) curves for copper

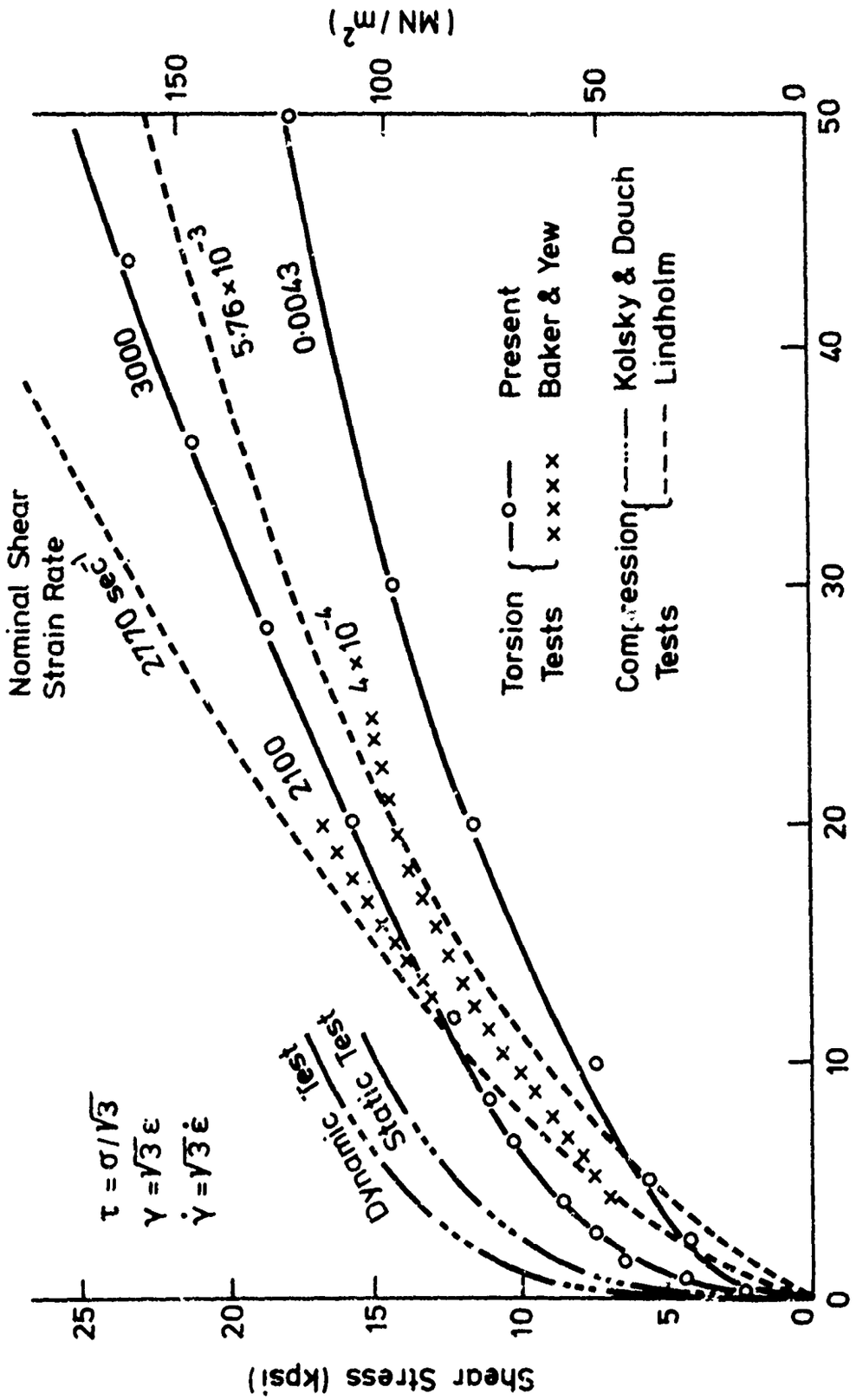

Fig. 6.5.6 Comparison of (τ, γ) curves for copper

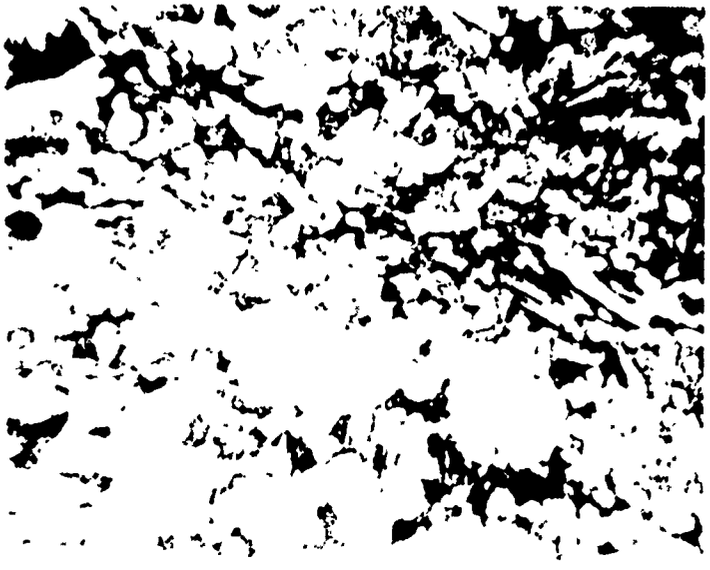

Fig. 6.6.1 Microstructure of brass, X113

(a) $t_k = 0.01856$ in. $r_m = 0.197$ in.
$\ell = 0.0486$ in. $\dot{\gamma} = 800 \quad sec^{-1}$

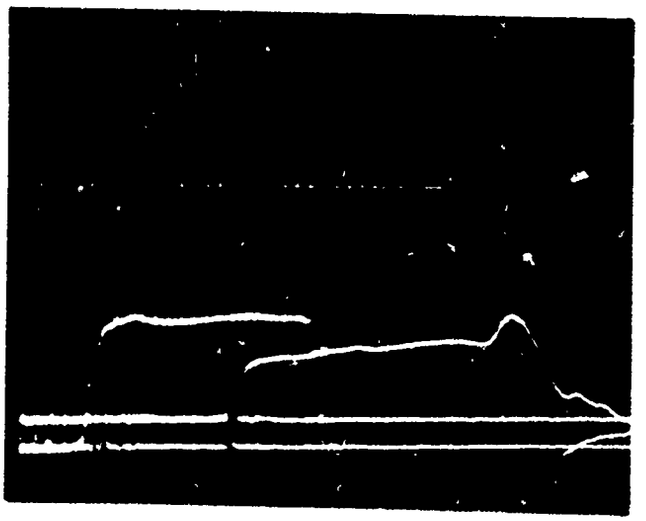

(b) $t_k = 0.0204$ in. $r_m = 0.1975$ in.
$\ell = 0.049$ in. $\dot{\gamma} = 1200 \quad sec^{-1}$

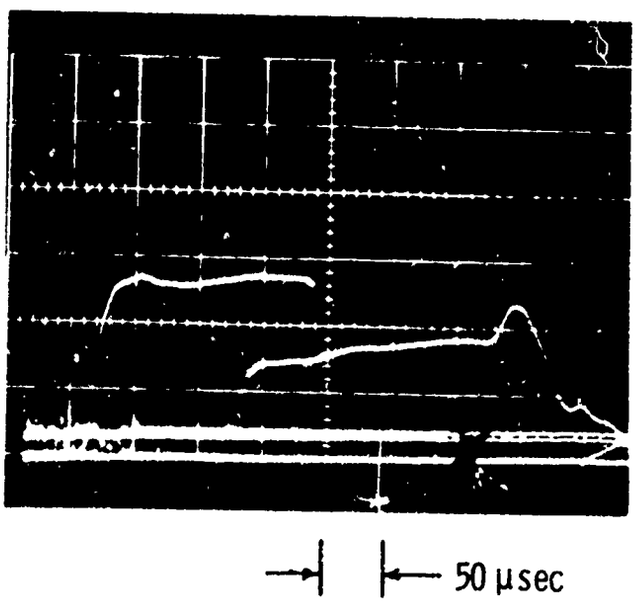

Fig. 6.6.2 Typical oscillograms for brass

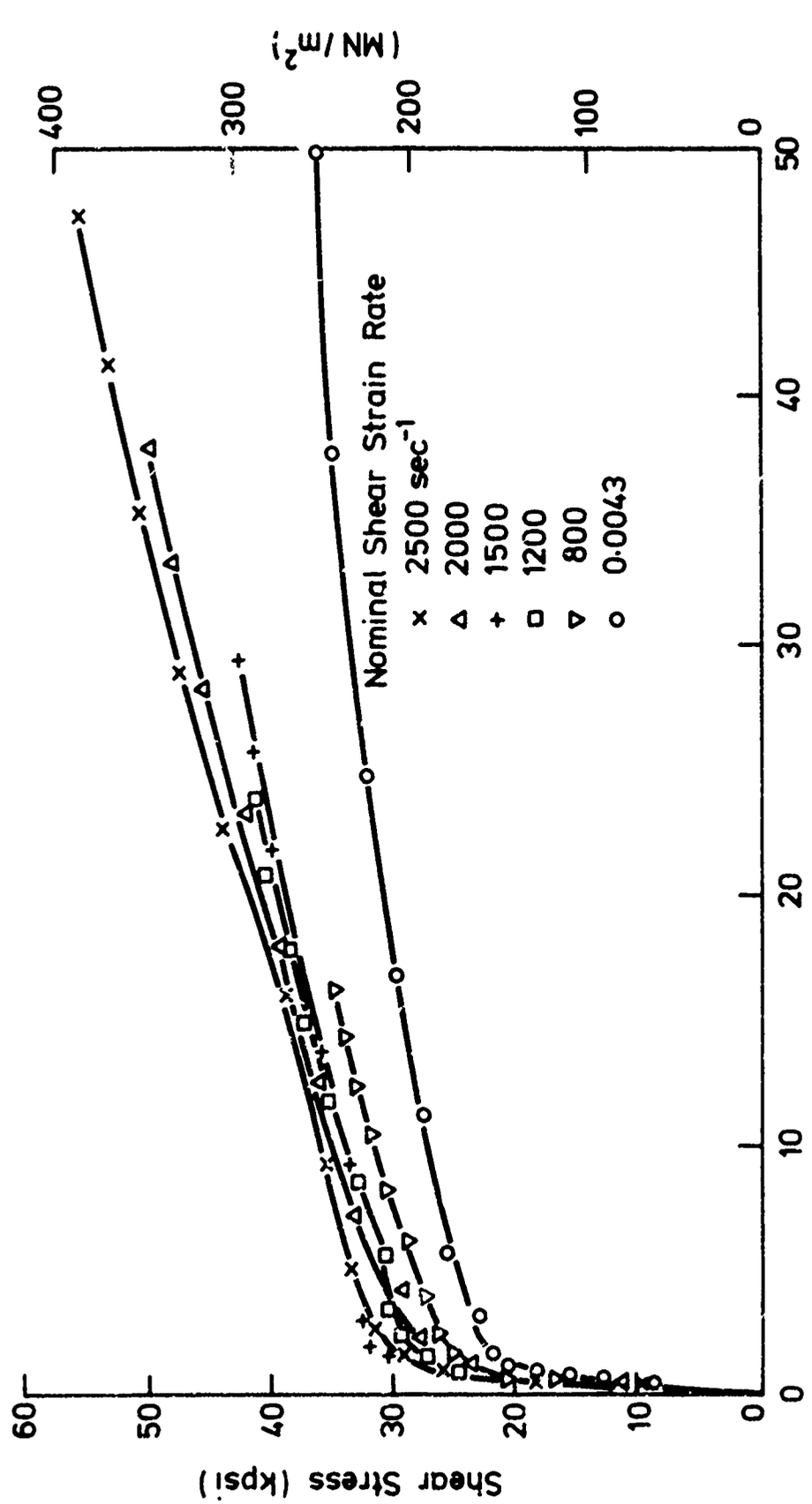

Fig. 4.6.3 (τ,γ) curves for yellow brass

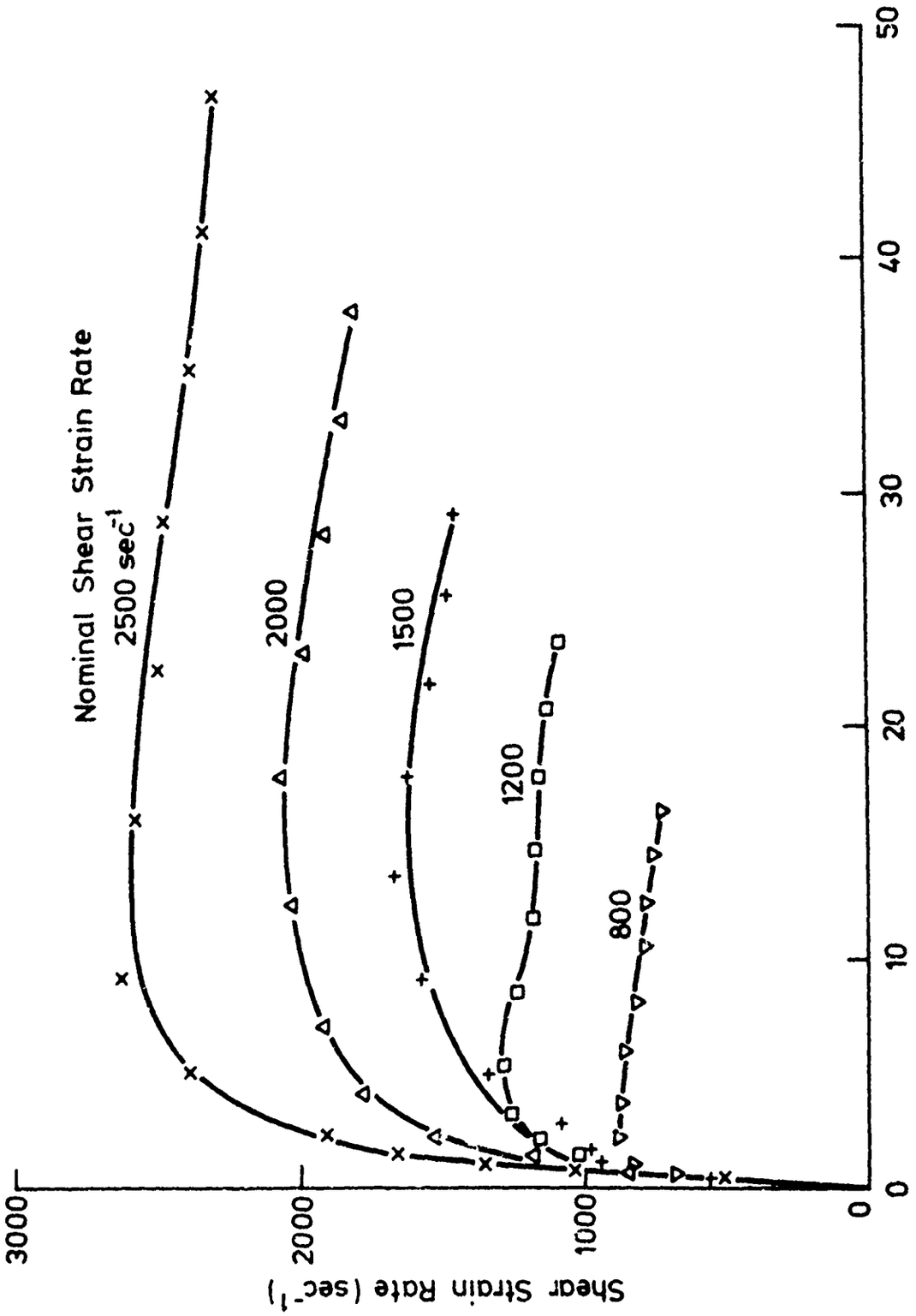

Fig. 6.6.4 (...) curves for yellow brass

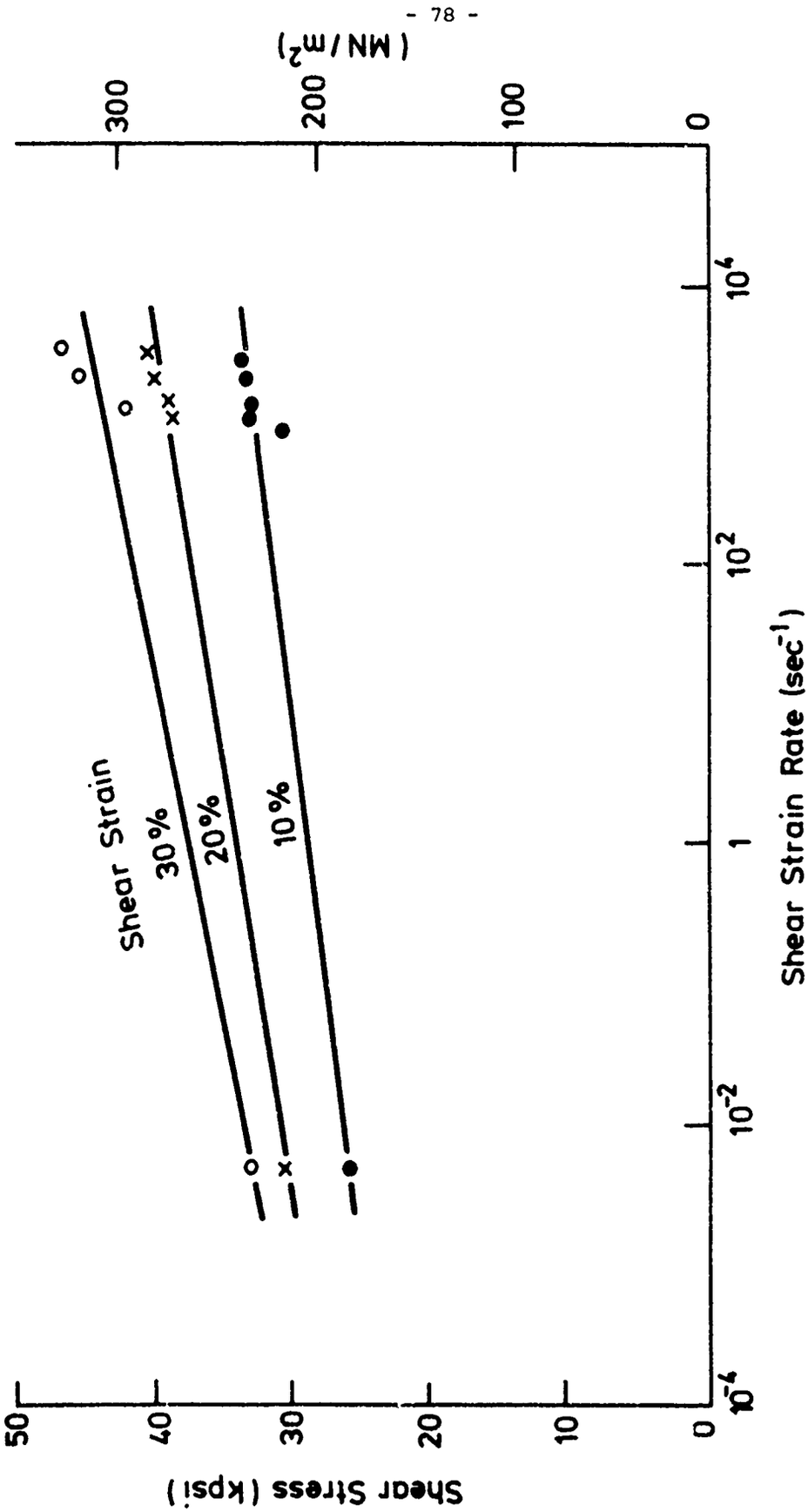

Fig. 6.6.5 (·, log $\dot{\gamma}$) curves for yellow brass

(a) $t_k = 0.0196$ in. $r_m = 0.198$ in.

$\ell = 0.0485$ in. $\dot{\gamma} = 1600 \quad sec^{-1}$

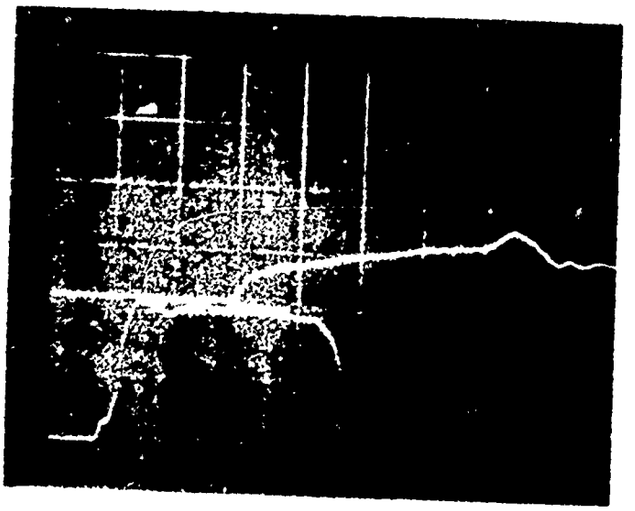

(b) $t_k = 0.0199$ in. $r_m = 0.1984$ in.

$\ell = 0.0503$ in. $\dot{\gamma} = 2200 \quad sec^{-1}$

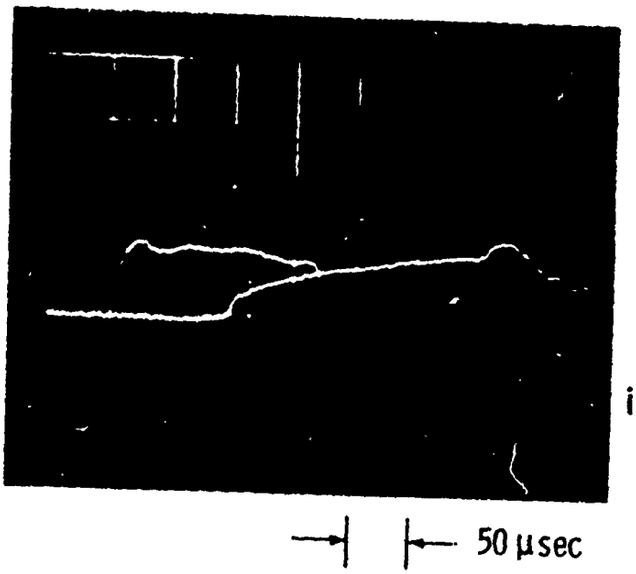

Fig. 6.7.1 Typical oscillograms for aluminium

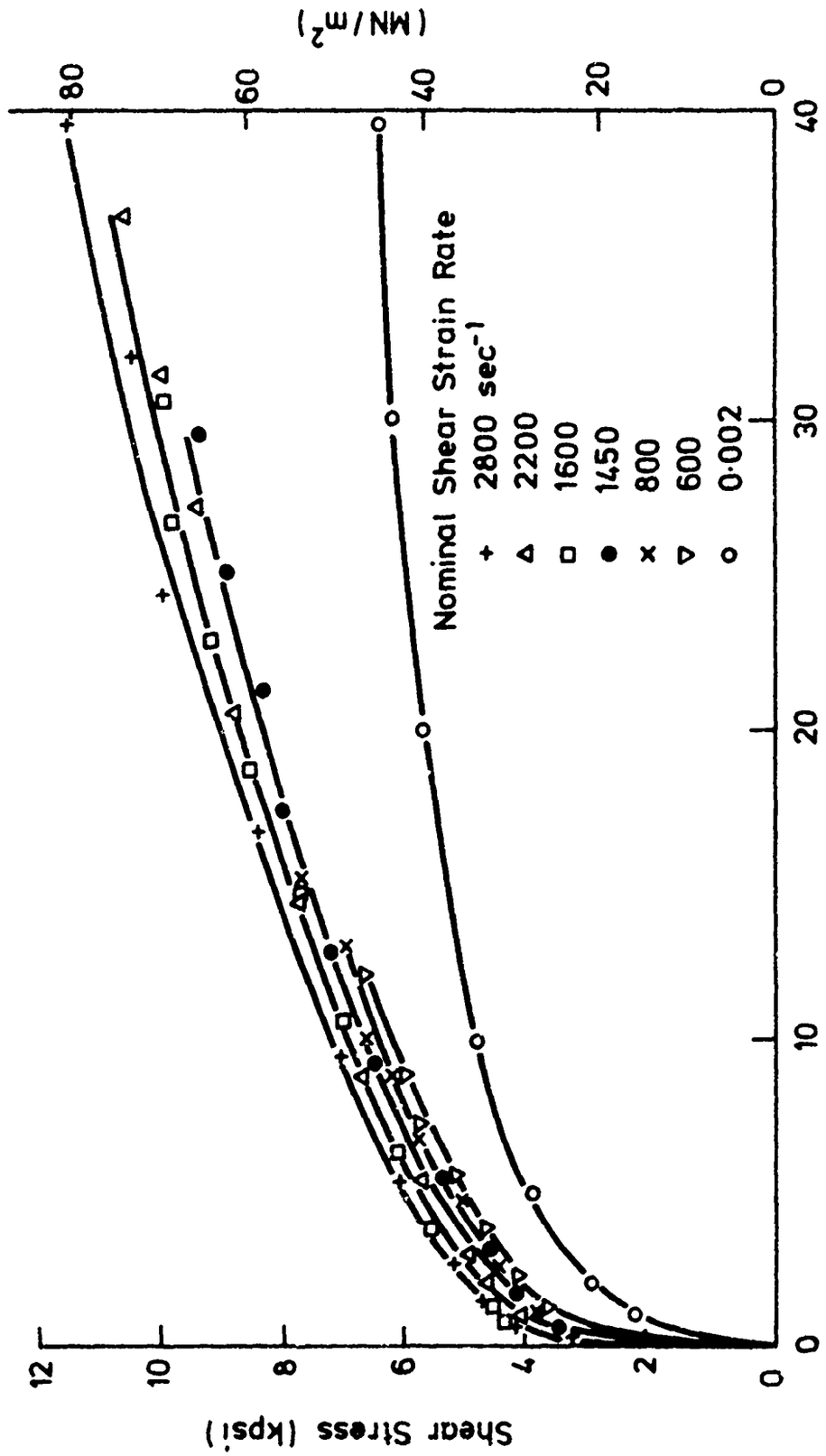

Fig. 6.7.2 (τ,γ) curves for aluminium

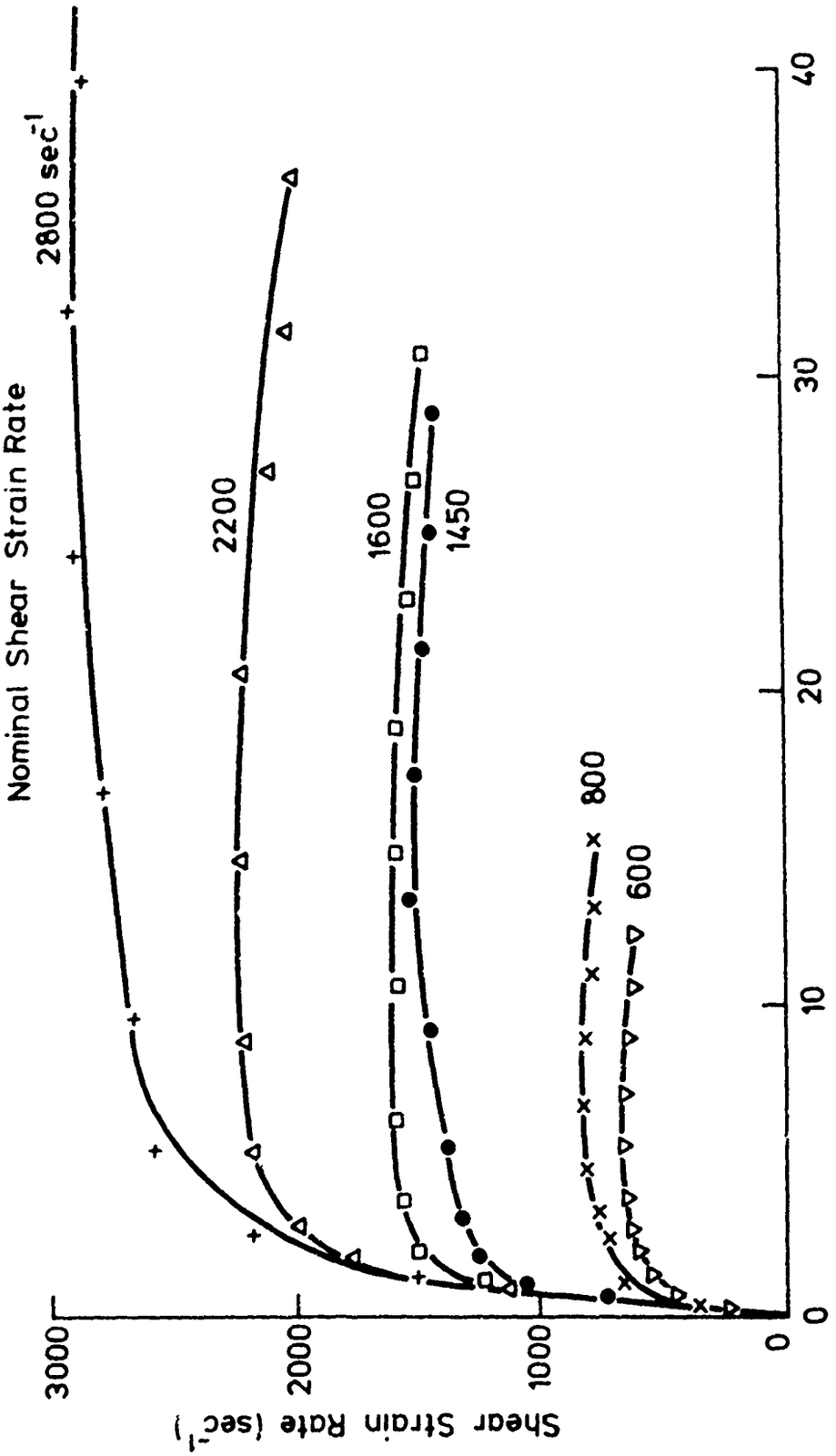

Fig. 6.7.3 $(\dot{\gamma},\gamma)$ curves for aluminium

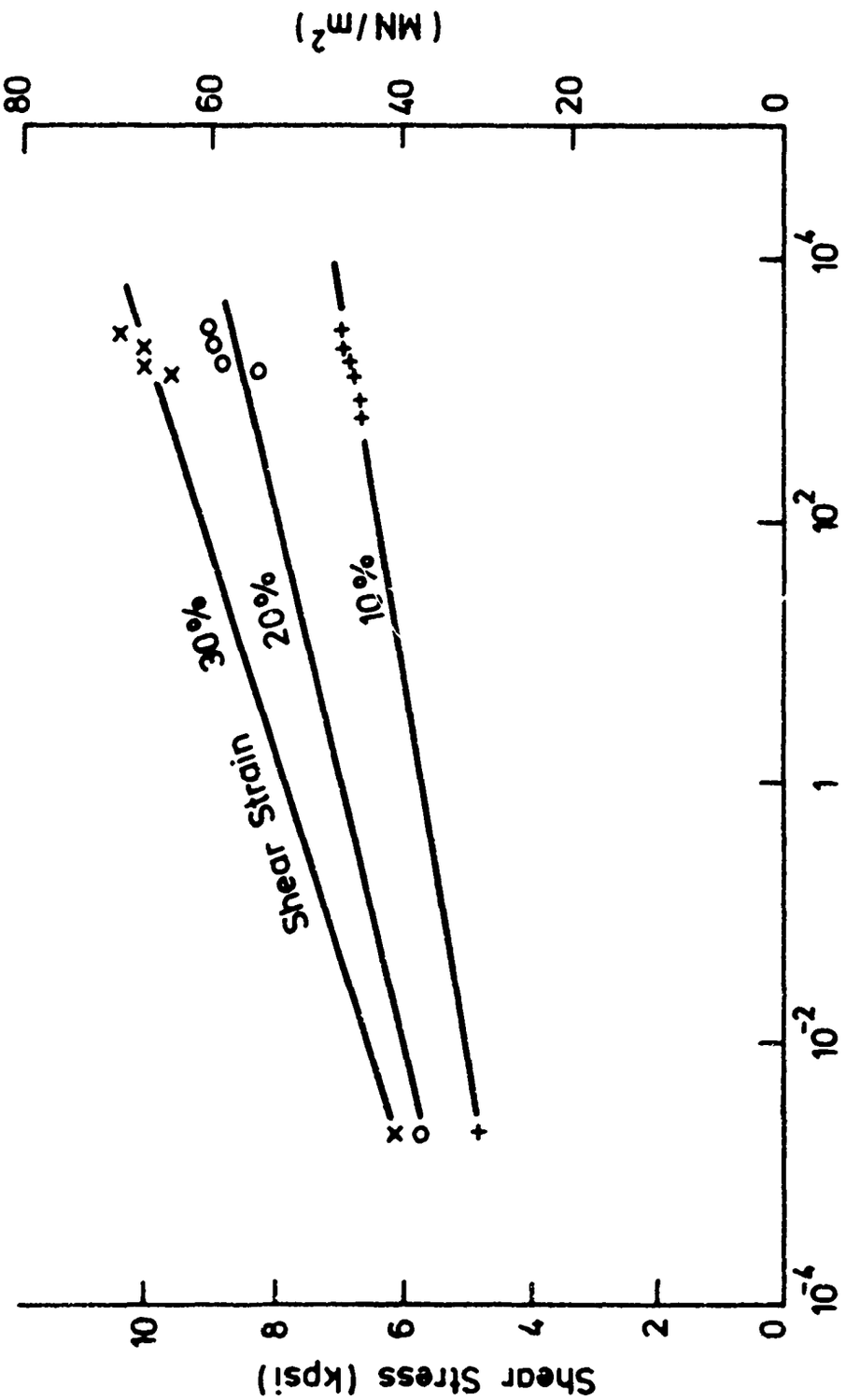

Fig. 6.7.4 (τ, log $\dot{\gamma}$) curves for aluminium

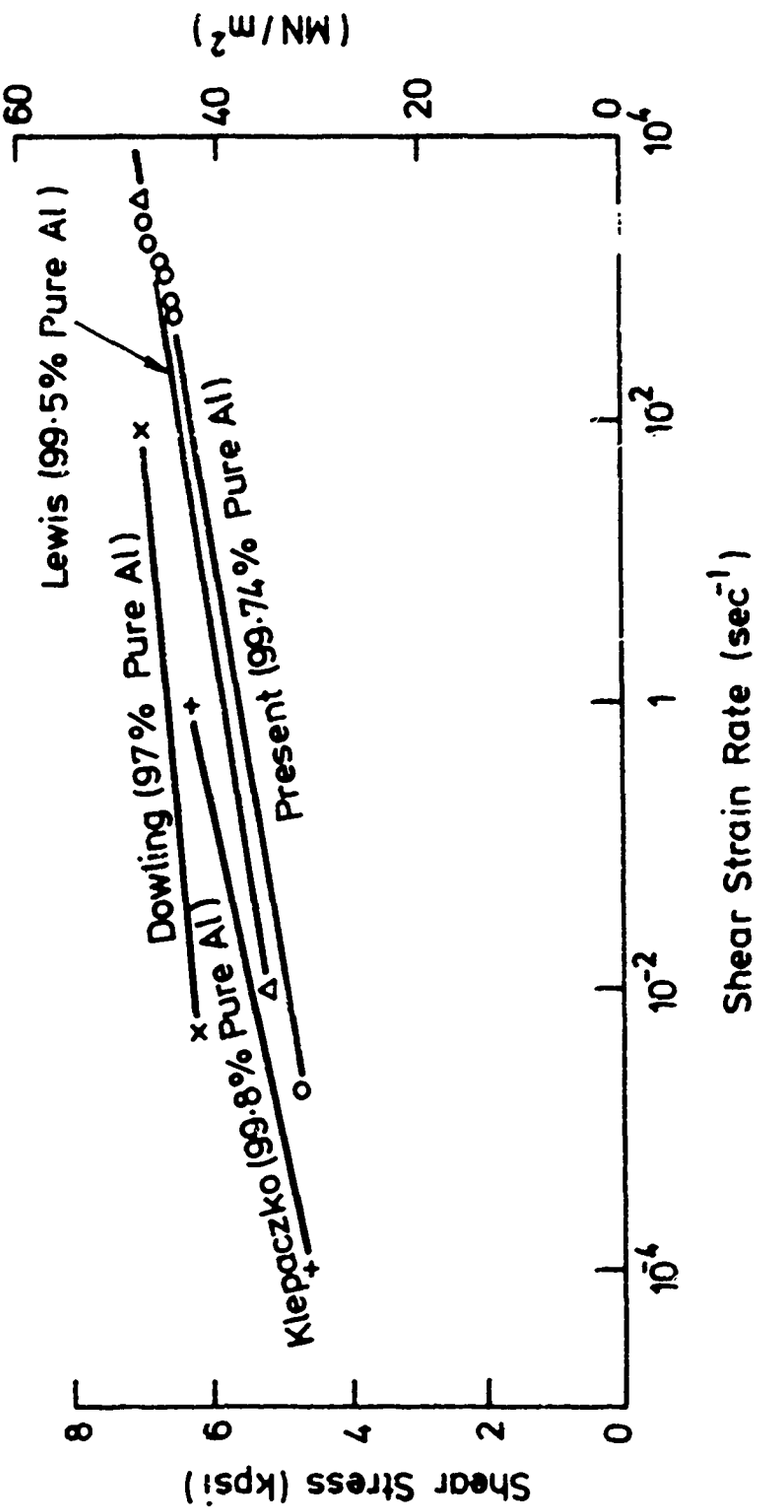

Fig. 6.7.5 Comparison flow stress results for aluminium at ε = 10%